

# Giant resonances in $^{40,48}\text{Ca}$ , $^{68}\text{Ni}$ , $^{90}\text{Zr}$ , $^{116}\text{Sn}$ , $^{144}\text{Sm}$ , and $^{208}\text{Pb}$

G. Bonasera,\* M. R. Anders, and S. Shlomo

*Cyclotron Institute, Texas A&M University, College Station, Texas 77843, USA*

(Received 18 July 2018; revised manuscript received 21 August 2018; published 26 November 2018)

We present results of centroid energies  $E_{\text{CEN}}$ , of the isoscalar ( $T = 0$ ) and isovector ( $T = 1$ ) giant resonances of multiplicities  $L = 0-3$  in  $^{40,48}\text{Ca}$ ,  $^{68}\text{Ni}$ ,  $^{90}\text{Zr}$ ,  $^{116}\text{Sn}$ ,  $^{144}\text{Sm}$ , and  $^{208}\text{Pb}$ , calculated within the fully self-consistent Hartree-Fock-based random phase approximation theory, using 33 different Skyrme-type effective nucleon-nucleon interactions of the standard form commonly adopted in the literature. We compare the results of our theoretical calculations with the available experimental data. We also study the sensitivity of the calculated  $E_{\text{CEN}}$  to physical properties of nuclear matter (NM), such as effective mass  $m^*/m$ , nuclear matter incompressibility coefficient  $K_{\text{NM}}$ , enhancement coefficient  $\kappa$  of the energy weighted sum rule for the isovector giant dipole resonance and symmetry energy at saturation density, associated with the Skyrme interactions used in the calculations. This is done by determining the Pearson linear correlation coefficient between the calculated  $E_{\text{CEN}}$  and a certain NM property. Constraining the values of the NM properties, by comparing the calculated values of  $E_{\text{CEN}}$  to the experimental data, we find that interactions associated with the values of  $K_{\text{NM}} = 210-240$  MeV and  $\kappa = 0.25-0.70$  best reproduce the experimental data.

DOI: [10.1103/PhysRevC.98.054316](https://doi.org/10.1103/PhysRevC.98.054316)

## I. INTRODUCTION

The phenomena of collective motion of strongly interacting nucleons in the many-body system of the atomic nucleus have been the subjects of experimental and theoretical investigations for many decades [1–3]. Of particular interest are the determination of properties of isoscalar (isospin  $T = 0$ ) and isovector ( $T = 1$ ) giant resonances of various multiplicities [1,2,4], evolution of astrophysical objects and the description of heavy-ion collisions (HICs) [5,6]. These studies are important for determining properties of the nucleon-nucleon interaction, nuclei, and infinite nuclear matter (NM). It is common to adopt a parametrized form for the energy density functional (EDF) for the nuclear many-body system and determine its parameters by a fit to ground-state properties of nuclei, such as binding energies and radii, and thereby determine the equation of state (EOS) of NM. Over the years the strength function distributions  $S(E)$  and centroid energies,  $E_{\text{CEN}}$ , of the isoscalar and isovector giant resonances have been found to be sensitive to physical quantities of NM [4,5,7,8], such as the incompressibility coefficient  $K_{\text{NM}}$  and symmetry energy,  $E_{\text{sym}}(\rho)$ , as a function of the density  $\rho$ . Many attempts have been made to determine the values of the bulk properties of NM. The resulting values of the bulk properties of NM can also be used to constrain the EDF, which then can be used to better determine the EOS of NM and calculate properties of nuclei away from the valley of stability.

The first observation of giant resonance dates back to 1947 made by Baldwin and Klaiber [9] by bombarding targets of uranium and thorium with  $\gamma$  rays from the newly

developed 100-MeV betatron. They found a strong peak in the photofission cross section: the isovector giant dipole resonance (IVGDR). With the use of inelastic proton and electron scattering experiments on nuclei, the isoscalar giant quadrupole resonance (ISGQR) was determined over two decades later, see Refs. [10,11]. Youngblood *et al.* found the isoscalar giant monopole resonance (ISGMR) in  $^{144}\text{Sm}$  and  $^{208}\text{Pb}$  using inelastic  $\alpha$  scattering and angular coverage close to  $0^\circ$  [12], and subsequently lead the systematic study of the strength distributions of isoscalar giant resonances in many other nuclei.

In this work we consider the isoscalar ( $T = 0$ ) and isovector ( $T = 1$ ) giant resonances, of multiplicities  $L = 0-3$  in  $^{40,48}\text{Ca}$ ,  $^{68}\text{Ni}$ ,  $^{90}\text{Zr}$ ,  $^{116}\text{Sn}$ ,  $^{144}\text{Sm}$ , and  $^{208}\text{Pb}$  and present results of calculations of the centroid energies  $E_{\text{CEN}}$ , within fully self-consistent spherical Hartree-Fock (HF)-based random phase approximation (RPA) theory, including all the particle-hole components of the Coulomb and the adopted effective nucleon-nucleon Skyrme type interactions [13–15]. Over the past decades, many parametrized Skyrme interactions have been obtained [16,17] by fitting the HF results to experimental data of ground-state properties of nuclei. In the following we present results for  $E_{\text{CEN}}$  using 33 Skyrme-type effective nucleon-nucleon interactions of the standard form [18], which cover a wide range of values of NM properties and commonly employed in the literature. We compare the calculated values of  $E_{\text{CEN}}$  with experimental data, obtained from different experiments carried out over a wide time frame; however, when possible we use data from the same experimental group for a better comparison. We also calculate the Pearson linear correlation coefficient to investigate the sensitivity of the  $E_{\text{CEN}}$  to bulk properties of NM including: the incompressibility

\* giacomo90@email.tamu.edu

TABLE I. Parameters for Skyrme interactions, units:  $t_0$  (MeV fm<sup>3</sup>),  $t_1$  (MeV fm<sup>5</sup>),  $t_3$  (MeV fm<sup>3(α+1)</sup>),  $W_0$  (MeV), and the remaining parameters are dimensionless.

Force	$t_0$	$t_1$	$t_2$	$t_3$	$W_0$	$x_0$	$x_1$	$x_2$	$x_3$	$X_w$	$\alpha$
SGII	-2645.00	340.00	-41.90	15595.00	105.00	0.0900	-0.0588	1.4250	0.0604	1.0000	1/6
KDE0	-2526.51	430.94	-398.38	14235.52	128.96	0.7583	-0.3087	-0.9495	1.1445	1.0000	0.1676
KDE0v1	-2553.08	411.70	-419.87	14603.61	124.41	0.6483	-0.3472	-0.9268	0.9475	1.0000	0.1673
SKM*	-2645.00	410.00	-135.00	15595.00	130.00	0.0900	0.0000	0.0000	0.0000	1.0000	1/6
SK255	-1689.35	389.30	-126.07	10989.60	95.39	-0.1461	0.1660	0.0012	-0.7449	1.0000	0.3563
SKI3	-1762.88	561.61	-227.09	8106.20	188.51	0.3083	-1.1722	-1.0907	1.2926	0.0000	1/4
SKI4	-1885.83	473.83	1006.86	9703.61	366.19	0.4051	-2.8891	-1.3252	1.1452	-0.9850	1/4
SKI5	-1772.91	550.84	-126.69	8206.25	123.63	-0.1171	-1.3088	-1.0487	0.3410	1.0000	1/4
SV-bas	-1879.64	313.75	112.68	12527.38	124.63	0.2585	-0.3817	-2.8236	0.1232	0.5474	0.3000
SV-min	-2112.25	295.78	142.27	13988.57	111.29	0.2439	-1.4349	-2.6259	0.2581	0.8255	0.2554
SV-sym32	-1883.28	319.18	197.33	12559.47	132.75	0.0077	-0.5943	-2.1692	-0.3095	0.4019	0.3
SV-m56-O	-1905.40	571.19	1594.80	8439.04	133.27	0.6440	-2.9737	-1.2553	1.7966	0.7949	0.2000
SV-m64-O	-2083.86	484.60	1134.35	10720.67	113.97	0.6198	-2.3327	-1.3059	1.2101	1.1042	0.2000
SLy4	-2488.91	486.82	-546.39	13777.00	123.00	0.8340	-0.3440	-1.0000	1.3540	1.0000	1/6
SLy5	-2484.88	483.13	-549.40	13763.00	126.00	0.7780	-0.3280	-1.0000	1.2670	1.0000	1/6
SLy6	-2479.50	462.18	-448.61	13673.00	122.00	0.8250	-0.4650	-1.0000	1.3550	1.0000	1/6
SkMP	-2372.24	503.62	57.28	12585.30	160.00	-0.1576	-0.4029	-2.9557	-0.2679	1.0000	1/6
SkO	-2103.65	303.35	791.67	13553.25	353.16	-0.2107	-2.8108	-1.4616	-0.4299	-1.1256	1/4
SkO'	-2099.42	301.53	154.78	13526.46	287.79	-0.0295	-1.3257	-2.3234	-0.1474	-0.5760	1/4
LNS	-2484.97	266.74	-337.14	14588.20	96.00	0.0628	0.6585	-0.9538	-0.0341	1.0000	0.1667
MSL0	-2118.06	395.20	-63.95	12857.70	133.30	-0.0709	-0.3323	1.3583	-0.2282	1.0000	0.2359
NRAPR	-2719.70	417.64	-66.69	15042.00	41.96	0.1615	-0.0480	0.0272	0.1361	1.0000	0.1442
SQMC650	-2462.70	436.10	-151.90	14154.50	110.50	0.1300	0.0000	0.0000	0.0000	1.3899	0.1667
SQMC700	-2429.10	371.00	-96.70	13773.60	104.60	0.1000	0.0000	0.0000	0.0000	1.3910	0.1667
SKT1	-1794.00	298.00	-298.00	12812.00	110.00	0.1540	-0.5000	-0.5000	0.0890	1.0000	1/3
SKT2	-1791.60	300.00	-300.00	12792.00	120.00	0.1540	-0.5000	-0.5000	0.0890	1.0000	1/3
SKT3	-1791.80	298.50	-99.50	12794.00	126.00	0.1380	-1.0000	1.0000	0.0750	1.0000	1/3
SKT8	-1892.50	367.00	-228.76	11983.00	109.00	0.4480	-0.5000	-0.5000	0.6950	1.0000	0.2850
SKT9	-1891.40	377.40	-239.16	11982.00	130.00	0.4410	-0.5000	-0.5000	0.6860	1.0000	0.2850
SKT1*	-1800.50	296.00	-296.00	12884.00	95.00	0.1570	-0.5000	-0.5000	0.0920	1.0000	1/3
SKT3*	-1800.50	296.00	-98.67	12884.00	95.00	0.1420	-1.0000	1.0000	0.0760	1.0000	1/3
Skxs20	-2885.24	302.73	-323.42	18237.49	162.73	0.1375	-0.2555	-0.6074	0.0543	0.0000	1/6
Z <sub>σ</sub>	-1983.76	362.25	-104.27	11861.40	123.69	1.1717	0.0000	0.0000	1.7620	1.0000	1/4

coefficient  $K_{NM} = 9\rho_0^2 \frac{\partial^2 E_0}{\partial \rho^2} |_{\rho_0}$ , where  $E_0[\rho]$  is the binding energy per nucleon and  $\rho_0$  is the saturation density, the effective mass  $m^*/m$ , the symmetry energy coefficients at  $\rho_0$ :  $J = E_{\text{sym}}[\rho_0]$ , and its first and second derivatives  $L = 3\rho_0 \frac{\partial E_{\text{sym}}}{\partial \rho} |_{\rho_0}$  and  $K_{\text{sym}} = 9\rho_0^2 \frac{\partial^2 E_{\text{sym}}}{\partial \rho^2} |_{\rho_0}$ , respectively, and  $\kappa$ , the enhancement coefficient of the energy weighted sum rule (EWSR) of the isovector giant dipole resonance (IVGDR). We consider spherical nuclei with a wide range of mass to determine better constraints on the values of various NM properties, associated with the standard form of the Skyrme interaction adopted in this investigation.

In Sec. II, we present the theoretical approach to calculate the centroid energies  $E_{\text{CEN}}$  of the giant resonances. In Sec. III, the calculated values of  $E_{\text{CEN}}$  are compared with the experimental data for each multipolarity. Here we also study the sensitivity of  $E_{\text{CEN}}$  to NM properties. Our summary and conclusions are given in Sec. IV.

## II. FORMALISM

The Skyrme effective nucleon-nucleon interactions used in our calculations have the standard form [18]

$$\begin{aligned}
V_{ij} = & t_0(1 + x_0 P_{ij}^\sigma) \delta(\vec{r}_i - \vec{r}_j) + \frac{1}{2} t_1 (1 + x_1 P_{ij}^\sigma) \\
& \times [\vec{k}_{ij}^2 \delta(\vec{r}_i - \vec{r}_j) + \delta(\vec{r}_i - \vec{r}_j) \vec{k}_{ij}^2] \\
& + t_2 (1 + x_2 P_{ij}^\sigma) \vec{k}_{ij} \delta(\vec{r}_i - \vec{r}_j) \vec{k}_{ij} \\
& + \frac{1}{6} t_3 (1 + x_3 P_{ij}^\sigma) \rho^\alpha \left( \frac{\vec{r}_i + \vec{r}_j}{2} \right) \delta(\vec{r}_i - \vec{r}_j) \\
& + i W_0 \vec{k}_{ij} \delta(\vec{r}_i - \vec{r}_j) (\vec{\sigma}_1 + \vec{\sigma}_2) \times \vec{k}_{ij}. \quad (1)
\end{aligned}$$

In Eq. (1),  $t_i$ ,  $x_i$ ,  $W_0$ , and  $\alpha$  are the 10 parameters of the Skyrme interaction.  $P_{ij}^\sigma$  is the spin exchange operator, and  $\vec{\sigma}_i$  is the Pauli spin operator. The momentum operators are

TABLE II. Same as Table I with the following conditions defining the interactions: HBTM = 0, 1, and 2, for  $\frac{\hbar^2}{2m} = 20.7525 \text{ MeV fm}^2$  for neutron and proton,  $\hbar^2/2m = 20.7213 \text{ MeV fm}^2$  for proton and  $\hbar^2/2m = 20.7498 \text{ MeV fm}^2$  for neutron, and  $\hbar^2/2m = 20.7355 \text{ MeV fm}^2$  for neutron and proton, respectively; JTM, contribution to the spin-orbit potential from  $t1$  and  $t2$  is taken for 1 and not for 0; CEX, Coulomb exchange on for 1 and off for 0; RHOC, proton density is used for Coulomb potential for 0 and charge density is used for Coulomb potential for 1; ZPE, center-of-mass correction is taken as  $(1 - 1/A)$  factor on the mass for 0 and is computed explicitly *a posteriori* as  $E_{\text{c.m.}} = \frac{1}{2mA} \langle \hat{P}^2 \rangle$  for 1.

Force	Ref.	HBTM	JTM	CEX	RHOC	ZPE
SGII	[24]	0	0	1	0	0
KDE0	[25]	2	1	0	0	1
KDE0v1	[25]	2	1	0	0	1
SKM*	[26]	0	0	1	0	0
SK255	[27]	2	1	0	0	1
SkI3	[28]	0	0	1	0	1
SkI4	[28]	0	0	1	0	1
SkI5	[28]	0	0	1	0	1
SV-bas	[29]	1	0	1	0	1
SV-min	[29]	1	0	1	0	1
SV-sym32	[29]	1	0	1	0	1
SV-m56-O	[30]	1	0	1	0	1
SV-m64-O	[30]	1	0	1	0	1
SLy4	[31]	2	0	1	0	0
SLy5	[31]	2	1	1	0	0
SLy6	[31]	2	0	1	0	1
SkMP	[32]	0	0	1	0	0
SkO	[33]	2	0	1	0	1
SkO'	[33]	2	1	1	0	1
LNS	[34]	2	0	1	0	0
MSL0	[35]	2	1	0	0	1
NRAPR	[36]	2	1	1	0	1
SQMC650	[37]	2	0	1	0	0
SQMC700	[37]	2	0	1	0	0
SkT1	[38]	1	1	1	1	0
SkT2	[38]	1	1	1	1	0
SkT3	[38]	1	1	1	1	0
SkT8	[38]	1	1	1	1	0
SkT9	[38]	1	1	1	1	0
SkT1*	[38]	1	1	1	1	0
SkT3*	[38]	1	1	1	1	0
Skxs20	[39]	0	1	0	0	1
Z $_{\sigma}$	[40]	0	1	1	0	1

defined by  $\vec{k}_{ij} = -\frac{i(\vec{\nabla}_i - \vec{\nabla}_j)}{2}$  and  $\overleftarrow{k}_{ij} = -\frac{i(\vec{\nabla}_i - \vec{\nabla}_j)}{2}$ , where the direction of the arrow indicates in what direction they act, right and left, respectively. The parameters of the effective nucleon-nucleon Skyrme interaction in Eq. (1) are generally determined by a fit of results of HF calculations to experimental data of ground-state properties, such as binding energies and radii of a wide range of nuclei. The corresponding energy

TABLE III. Excitation energy range  $E1-E2$  (in MeV) for calculating the centroid energies of the isoscalar and isovector giant resonances from the corresponding strength functions.

	$^{40}\text{Ca}$	$^{48}\text{Ca}$	$^{68}\text{Ni}$	$^{90}\text{Zr}$	$^{116}\text{Sn}$	$^{144}\text{Sm}$	$^{208}\text{Pb}$
L0T0	7-60	7-60	7-60	7-60	7-60	7-60	7-60
L1T0	20-60	20-60	20-60	20-60	16-60	16-60	16-60
L2T0	7-60	7-60	7-60	7-60	7-60	7-60	7-60
L3T0	20-60	20-60	20-60	15-60	15-60	15-60	15-60
L0T1	7-60	7-60	7-60	7-60	7-60	7-60	7-60
L1T1	0-60	0-60	0-60	0-60	0-60	0-60	0-60
L2T1	7-60	7-60	7-60	7-60	7-60	7-60	7-60
L3T1	25-60	25-60	25-60	25-60	25-60	25-60	25-60

density functional can be written as the sum of the individual components [18],

$$H = K + H_I = K + H_0 + H_3 + H_{\text{eff}} + H_{\text{fin}} + H_{so} + H_{sg} + H_{\text{Coul}}. \quad (2)$$

In the right-hand side (r.h.s.) of (2),  $K = \frac{\hbar^2}{2m} \tau$  is the kinetic term,  $H_0$  the zero-range term,  $H_3$  the density-dependent term,  $H_{\text{eff}}$  the effective mass term,  $H_{\text{fin}}$  the finite-range term,  $H_{so}$  the spin orbit term,  $H_{sg}$  the term due to tensor coupling with spin and gradient, and  $H_{\text{Coul}}$  is the Coulomb term. From Eq. (1) one finds that:

$$H_0 = \frac{1}{4} t_0 [(2 + x_0) \rho^2 - (2x_0 + 1)(\rho_p^2 + \rho_n^2)], \quad (3)$$

$$H_3 = \frac{1}{24} t_3 \rho^\alpha [(2 + x_3) \rho^2 - (2x_3 + 1)(\rho_p^2 + \rho_n^2)], \quad (4)$$

$$H_{\text{eff}} = \frac{1}{8} [t_1(2 + x_1) + t_2(2 + x_2)] \tau \rho + \frac{1}{8} [t_2(2x_2 + 1) - t_1(2x_1 + 1)] (\tau_p \rho_p + \tau_n \rho_n), \quad (5)$$

$$H_{\text{fin}} = \frac{1}{32} [3t_1(2 + x_1) - t_2(2 + x_2)] (\vec{\nabla} \rho)^2 - \frac{1}{32} [3t_1(2x_1 + 1) + t_2(2x_2 + 1)] [(\vec{\nabla} \rho_p)^2 + (\vec{\nabla} \rho_n)^2], \quad (6)$$

$$H_{so} = \frac{W_0}{2} [\vec{J} \cdot \vec{\nabla} \rho + x_w (\vec{J}_p \cdot \vec{\nabla} \rho_p + \vec{J}_n \cdot \vec{\nabla} \rho_n)], \quad (7)$$

and

$$H_{sg} = -\frac{1}{16} (t_1 x_1 + t_2 x_2) J^2 + \frac{1}{16} (t_1 - t_2) (J_p^2 + J_n^2), \quad (8)$$

where  $\rho = \rho_p + \rho_n$ ,  $\tau = \tau_p + \tau_n$  and  $\vec{J} = \vec{J}_p + \vec{J}_n$ , are the particle number density, the kinetic-energy density, and the spin density, respectively. The subscript  $p$  denotes the protons and  $n$  the neutrons [18]. The parameter  $x_w$  in Eq. (7) is introduced to tune the isospin dependence of the spin-orbit term.

The Coulomb contribution to the energy density functional can be written as a sum of two components, the direct and the exchange terms:

$$H_{\text{Coul}}(r) = H_{\text{Coul}}^{\text{dir}}(r) + H_{\text{Coul}}^{\text{ex}}(r). \quad (9)$$

TABLE IV. Nuclear matter (NM) properties of symmetric NM at nuclear saturation density associated with the Skyrme interactions of Table I. We have the saturation density  $\rho_0$  [fm<sup>3</sup>], the total binding energy per nucleon  $E/A$  [MeV], the incompressibility coefficient  $K_{\text{NM}}$  (MeV) of NM, the coefficients related to the symmetry energy density  $J$  (MeV),  $L$  (MeV), and  $K_{\text{sym}}$  (MeV), the isoscalar effective mass  $m^*/m$ , the enhancement factor of the EWSR of the IVGDR  $\kappa$ , the strength of the spin-orbit interaction  $W_0$  (MeV) and the Landau parameter  $G'_0$ .

Force	$\rho_0$	$E/A$	$K_{\text{NM}}$	$J$	$L$	$K_{\text{sym}}$	$m^*/m$	$\kappa$	$W_0$	$G'_0$
SGII	0.159	15.59	215.0	26.80	37.63	-145.90	0.79	0.49	105.00	0.5052
KDE0	0.161	16.11	228.8	33.00	45.22	-144.78	0.72	0.30	128.96	0.0474
KDE0v1	0.165	16.23	227.5	34.58	54.70	-127.12	0.74	0.23	124.41	0.0006
SKM*	0.160	15.78	216.7	30.03	45.78	-155.94	0.79	0.53	130.00	0.3142
SK255	0.157	16.33	255.0	37.40	95.00	-58.33	0.80	0.54	95.39	0.3733
SkI3	0.158	15.96	258.1	34.80	100.52	73.04	0.58	0.25	188.51	0.2035
SkI4	0.160	15.92	247.9	29.50	60.39	-40.56	0.65	0.25	366.19	1.3813
SkI5	0.156	15.83	255.7	36.70	129.33	159.57	0.58	0.25	123.63	0.3013
SV-bas	0.160	15.90	234.0	30.00	45.21	-221.75	0.90	0.40	124.63	0.7279
SV-min	0.161	15.91	222.0	30.01	44.76	-156.57	0.95	0.08	111.29	0.7963
SV-sym32	0.159	15.94	233.81	32.00	57.07	-148.79	0.90	0.40	132.745	0.8319
SV-m56-O	0.157	15.81	254.6	27.00	49.96	-45.04	0.56	0.60	133.27	1.6523
SV-m64-O	0.159	15.82	241.4	27.01	30.63	-144.76	0.64	0.60	113.97	1.4667
SLy4	0.160	15.97	229.9	32.00	45.96	-119.73	0.70	0.25	123.00	-0.1337
SLy5	0.160	15.98	229.9	32.03	48.27	-112.76	0.70	0.25	126.00	-0.1414
SLy6	0.159	15.92	229.8	31.96	47.44	-112.71	0.69	0.25	122.00	-0.0038
SKMP	0.157	15.56	230.9	29.88	70.31	-49.82	0.65	0.71	160.00	0.4653
SkO	0.160	15.84	223.34	31.97	79.14	-43.17	0.90	0.17	353.16	1.6191
SkO'	0.160	15.75	222.3	31.95	68.93	-78.82	0.90	0.15	287.79	0.7923
LNS	0.175	15.32	210.78	33.43	61.45	-127.36	0.83	0.38	96.00	0.1367
MSL0	0.160	16.00	230.00	30.00	60.00	-99.33	0.80	0.43	133.30	0.4160
NRAPR	0.161	15.85	225.65	32.78	59.63	-123.32	0.69	0.66	41.96	0.4100
SQMC650	0.172	15.57	218.11	33.65	52.92	-173.15	0.78	0.59	110.5	0.2018
SQMC700	0.171	15.49	222.20	33.47	59.06	-140.84	0.76	0.56	104.60	0.3600
SKT1	0.161	15.98	236.16	32.02	56.18	-134.83	1.00	0.00	110.00	0.1642
SKT2	0.161	15.94	235.73	32.00	56.16	-134.67	1.00	0.00	120.00	0.1573
SKT3	0.161	15.95	235.74	31.50	55.31	-132.05	1.00	0.00	126.00	0.4516
SKT8	0.161	15.94	235.70	29.92	33.72	-187.52	0.83	0.20	109.00	0.2386
SKT9	0.160	15.88	234.91	29.76	33.74	-185.62	0.83	0.20	130.00	0.2142
SKT1*	0.162	16.20	238.95	32.31	56.58	-136.66	1.00	0.00	95.00	0.1757
SKT3*	0.162	16.20	238.95	31.97	56.32	-133.65	1.00	0.00	95.00	0.4616
Skxs20	0.162	15.79	201.76	35.49	67.07	-122.25	0.96	0.08	162.73	0.1286
$Z_\sigma$	0.163	15.88	233.33	26.69	-29.38	-401.43	0.78	0.51	123.69	0.3951

The direct Coulomb term is given by

$$H_{\text{Coul}}^{\text{dir}}(r) = \frac{1}{2}e^2\rho_p(r) \int \frac{\rho_p(r')}{|r-r'|} d^3r', \quad (10)$$

while the exchange Coulomb term is commonly implemented using the Slater approximation

$$H_{\text{Coul}}^{\text{ex}}(r) = -\frac{3}{4}e^2\rho_p(r) \left[ \frac{3\rho_p(r)}{\pi} \right]^{1/3}. \quad (11)$$

The Hartree-Fock total energy  $E$  of the system and corresponding mean-field  $V_{HF}$  are found using

$$E = \int H(r)d^3r, \quad V_{HF} = \frac{\delta H}{\delta \rho}. \quad (12)$$

Within the RPA formalism the strength function  $S(E)$  is given by

$$S(E) = \sum_j | \langle 0 | F_L | j \rangle |^2 \delta(E_j - E_0), \quad (13)$$

where the sum is over all RPA states  $|j\rangle$  of energy  $E_j$ . The electromagnetic single-particle scattering operator for the isoscalar ( $T=0$ ) excitation of multipolarity  $L$  is given by [19]  $F_L = \sum_i f(r_i)Y_{L0}(i)$  and the corresponding isovector ( $T=1$ ) single-particle scattering operator is given by  $F_L = \frac{Z}{A} \sum_n f(r_n)Y_{L0}(n) - \frac{N}{A} \sum_p f(r_p)Y_{L0}(p)$ . The  $S(E)$  of the different multiplicities is then determined by:  $f(r) = r^2$ , for the isoscalar and isovector monopole ( $L=0$ ) and quadrupole ( $L=2$ ),  $f(r) = r^3$  for the octupole ( $L=3$ ),  $f(r) = r$  for the isovector dipole ( $T=1, L=1$ ), and lastly  $f(r) = r^3 - (5/3)\langle r^2 \rangle r$  for the isoscalar dipole ( $T=0, L=1$ ). We point

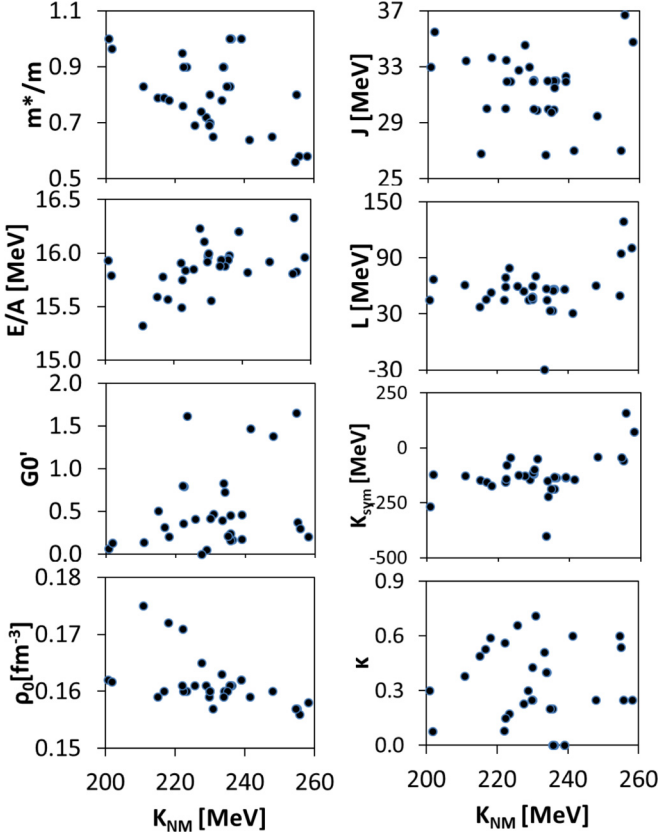


FIG. 1. Various NM properties of the Skyrme interactions are plotted against the incompressibility coefficient  $K_{\text{NM}}$ . In each panel, from top left to bottom, we have the effective mass  $m^*/m$ , the total binding energy per nucleon  $E/A$ , the Landau parameter  $G0'$ , the saturation density  $\rho_0$ , the symmetry energy at saturation density  $J$ , the first derivative of the symmetry energy  $L = 3\rho_0 \frac{\partial E_{\text{sym}}}{\partial \rho} |_{\rho_0}$ , the second derivative of the symmetry energy  $K_{\text{sym}} = 9\rho_0^2 \frac{\partial^2 E_{\text{sym}}}{\partial \rho^2} |_{\rho_0}$  and the enhancement coefficient  $\kappa$  of the IVGDR EWSR. We see no strong dependence for any of these parameters and  $K_{\text{NM}}$ , although a weak relation with  $m^*/m$  and  $\rho_0$  is still present.

out that for the isoscalar dipole we subtract the contribution from the spurious state [20,21].

We calculate the energy moments of the  $S(E)$  using,

$$m_k = \int_{E_1}^{E_2} E^k S(E) dE, \quad (14)$$

TABLE V. Pearson linear correlation coefficients for the values of pairs of nuclear properties associated with the 33 Skyrme effective nucleon-nucleon interactions of Table I.

	$K_{\text{NM}}$	$J$	$L$	$K_{\text{sym}}$	$m^*/m$	$\kappa$	$W_0(X_W = 1)$
$K_{\text{NM}}$	1.00	0.03	0.30	0.43	-0.37	-0.02	0.03
$J$	0.03	1.00	0.72	0.49	0.07	-0.24	-0.25
$L$	0.30	0.72	1.00	0.91	-0.15	-0.13	-0.08
$K_{\text{sym}}$	0.43	0.49	0.91	1.00	-0.41	-0.08	0.05
$m^*/m$	-0.37	0.07	-0.15	-0.41	1.00	-0.63	-0.19
$\kappa$	-0.02	-0.24	-0.13	-0.08	-0.63	1.00	-0.03
$W_0(X_W = 1)$	0.03	-0.25	-0.08	0.05	-0.19	-0.03	1.00

where  $E_1$ – $E_2$  is the appropriate excitation energy range. The constrained, centroid, and scaling energies of the resonances are then obtained using

$$E_{\text{CON}} = \left( \frac{m_1}{m_{-1}} \right)^{1/2},$$

$$E_{\text{CEN}} = \frac{m_1}{m_0} \quad \text{and} \quad E_s = \left( \frac{m_3}{m_1} \right)^{1/2}. \quad (15)$$

We note that the energy moment  $m_1$  in Eq. (14), calculated by integrating over all excitation energies, can be also determined directly from using only the HF ground-state wave function, thus leading to an energy weighted sum rule (EWSR) for  $S(E)$  [1,22]. The EWSR for the isoscalar ( $T = 0$ )  $F_L$  operator is given by:

$$m_1(L, T = 0) = \frac{1}{4\pi} \frac{\hbar^2}{2m} \int g_L(r) \rho(r) 4\pi r^2 dr, \quad (16)$$

where  $\rho(r)$  is the HF ground-state matter density distribution and

$$g_L(r) = \left( \frac{df}{dr} \right)^2 + L(L+1) \left( \frac{f}{r} \right)^2. \quad (17)$$

For the isovector ( $T = 1$ ) operator  $F_L$ , the EWSR is given by

$$m_1(L, T = 1) = \frac{NZ}{A^2} m_1(L, T = 0) [1 + \kappa - \kappa_{np}]. \quad (18)$$

Here,  $\kappa$  is the EWSR enhancement coefficient of the isovector giant resonance of multipolarity  $L$  and is due to the momentum dependence of the effective nucleon-nucleon interaction. For the Skyrme interaction of Eq. (1) we have

$$\kappa = \frac{(1/2)[t_1(1+x_1/2) + t_2(1+x_1/2)]}{(\hbar^2/2m)(4NZ/A^2)} \times \frac{2 \int g_L(r) \rho_p(r) \rho_n(r) 4\pi r^2 dr}{\int g_L(r) \rho(r) 4\pi r^2 dr}, \quad (19)$$

where  $t_i$  and  $x_i$  are the parameters of the interaction. The coefficient  $\kappa_{np}$ , which is due to the difference in the profiles of the neutron and proton density distributions [i.e., when



TABLE VI. Pearson linear correlation coefficients between the calculated centroid energy of each giant resonance and each nuclear matter property at saturation density.

	$K_{\text{NM}}$	$J$	$L$	$K_{\text{sym}}$	$m^*/m$	$\kappa$	$W_0(X_W = 1)$
ISGMR	0.87	-0.10	0.25	0.45	-0.51	0.13	0.11
ISGDR	0.52	-0.10	0.13	0.36	-0.88	0.55	0.04
ISGQR	0.41	-0.09	0.15	0.41	-0.93	0.54	0.22
ISGOR	0.42	-0.10	0.15	0.43	-0.96	0.56	0.16
IVGMR	0.23	-0.26	-0.12	0.00	-0.70	0.86	-0.09
IVGDR	0.05	-0.37	-0.42	-0.30	-0.60	0.84	-0.06
IVGQR	0.18	-0.35	-0.29	-0.13	-0.74	0.80	0.00
IVGOR	0.25	-0.32	-0.19	0.02	-0.83	0.81	0.04

$\rho_n(r) - \rho_p(r) \neq \frac{N-Z}{A} \rho(r)$ , is determined from

$$\kappa_{np} = \frac{(N-Z)}{A} \frac{A}{NZ} \frac{\int g_L(r) [Z\rho_n(r) - N\rho_p(r)] 4\pi r^2 dr}{\int g_L(r) \rho(r) 4\pi r^2 dr}. \quad (20)$$

### III. RESULTS

In this section we present results of our spherical HF-based RPA calculations of the centroid energies  $E_{\text{CEN}}$  of isoscalar and isovector giant resonances of multipolarity  $L = 0-3$  in  $^{40,48}\text{Ca}$ ,  $^{68}\text{Ni}$ ,  $^{90}\text{Zr}$ ,  $^{116}\text{Sn}$ ,  $^{144}\text{Sm}$ , and  $^{208}\text{Pb}$ , obtained from the 33 Skyrme-type effective interactions of the standard form of Eq. [1], commonly employed in the literature. We use the occupation number approximation for the single-particle orbits for the open-shell nucleus  $^{144}\text{Sm}$ , to ensure a spherical nucleus, and we use all the interaction terms from the HF when we carry out the RPA calculations, for self-consistency [23]. The interactions used in this work are: SGII [24], KDE0 [25], KDE0v1 [25], SKM\* [26], SK255 [27], SkI3 [28], SkI4 [28], SkI5 [28], SV-bas [29], SV-min [29], SV-sym32 [29], SV-m56-O [30], SV-m64-O [30], SLy4 [31], SLy5 [31], SLy6 [31], SkMP [32], SkO [33], SkO' [33], LNS [34], MSL0 [35], NRAPR [36], SQMC650 [37], SQMC700 [37], SkT1 [38], SkT2 [38], SkT3 [38], SkT8 [38], SkT9 [38], SkT1\* [38], SkT3\* [38], Skxs20 [39], and  $Z\sigma$  [40]. A list of the parameters of each Skyrme interaction used here is presented in Table I. In Table II we show the different conditions for

TABLE VII. Experimental value for the centroid energies of isoscalar and isovector giant resonances. The data was taken from the following references: [45] for a, [46] for b, [44] for c, [47] for d, [48] for e, [22] for f, [52] for g, [53] for h, [54] for i, [55] for j, [56] for k, [57] for m, [58] for n, and [60] for p.

	$^{40}\text{Ca}$	$^{48}\text{Ca}$	$^{68}\text{Ni}$	$^{90}\text{Zr}$	$^{116}\text{Sn}$	$^{144}\text{Sm}$	$^{208}\text{Pb}$
L0T0	19.18 (37) a	19.88 (16) b	21.9 (19) c	17.88 (12) d	15.85 (20) e	15.40 (30) e	13.96 (20) e
L1T0	23.36 (70) a	27.30 (15) b		27.40 (50) d	25.50 (60) e	24.51 (40) e	22.20 (30) e
L2T0	17.84 (43) a	18.61 (24) b		14.56 (20) d	13.50 (35) e	12.78 (30) e	10.89 (30) e
L3T0				23.10 (30) d	23.30 (80) e	19.80 (50) e	19.60 (50) e
L0T1	31.0 (20) f						26.00 (2.0) f
L1T1	19.80 (50) g	19.50 (50) i	17.10 (20) j	16.83 (04) k	15.67 (04) m	15.30 (10) n	13.40 (50) p
L2T1	31.0 (15) h						22.80 (50) f

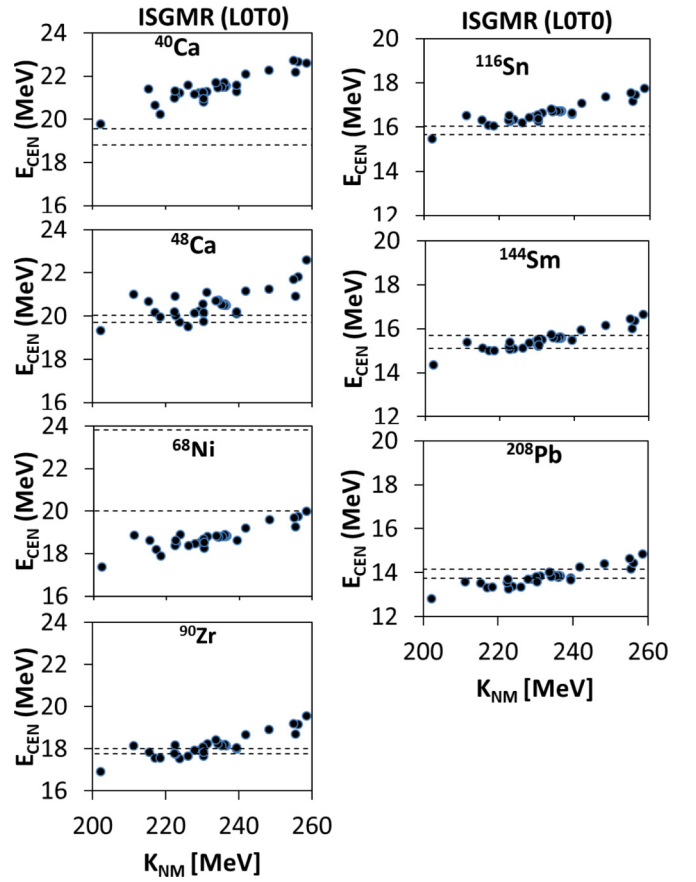


FIG. 2. Calculated centroid energies  $E_{\text{CEN}}$  in MeV (full circle) of the isoscalar giant monopole resonances (ISGMR) for the different interactions, as a function of the incompressibility coefficient  $K_{\text{NM}}$ . Each nucleus has its own panel and the experimental uncertainties are contained by the dashed lines. As expected we find strong correlation between the calculated values of  $E_{\text{CEN}}$  and  $K_{\text{NM}}$  with a Pearson linear correlation coefficient  $C \sim 0.87$ .

using each Skyrme interaction as it was designed. The strength functions  $S(E)$ , Eq. (13), for all the giant resonances in all nuclei, have been calculated using the discretized RPA method described in Ref. [19]. In all the calculations of  $S(E)$ , we use the same sized box of 100 mesh points, 0.2 fm apart. In the RPA calculations the maximum cutoff single-particle energy

was varied only for the different multiplicities, with 100, 80, 45, and 45 MeV used for  $L = 0, 1, 2,$  and  $3$ , respectively. Our calculated values for the centroid energies  $E_{\text{CEN}}$  were obtained from Eq. (14) using the excitation energy ranges given in Table III, determined by studying the structure of the corresponding strength functions in order to obtain accurate values for  $E_{\text{CEN}}$ . We have checked that the cutoff energies are large enough, so that the corresponding energy weighted sum rules are exhausted and that the calculated values of  $E_{\text{CEN}}$  are accurate within 0.1 MeV, by repeating the calculations using 200 mesh points with mesh size of 0.1 fm for several isoscalar and isovector giant resonances (see also Ref. [23]). To ensure accuracy in the integration of the strength function, Eq. (13), when obtaining the energy moments, we use a small parameter ( $\gamma = 0.1$  MeV) in the Lorentzian smearing of the strength function.

In Table IV we present the values of the nuclear matter (NM) properties associated with the 33 interactions used in this work. In Fig. 1, we show the range of the NM properties relative to these interactions as a function of the incompressibility coefficient,  $K_{\text{NM}}$ , of NM. It is seen from Table IV and Fig. 1 that the interactions used in this work cover wide ranges of values for the properties of NM. We calculated the Pearson linear correlation coefficients between the values

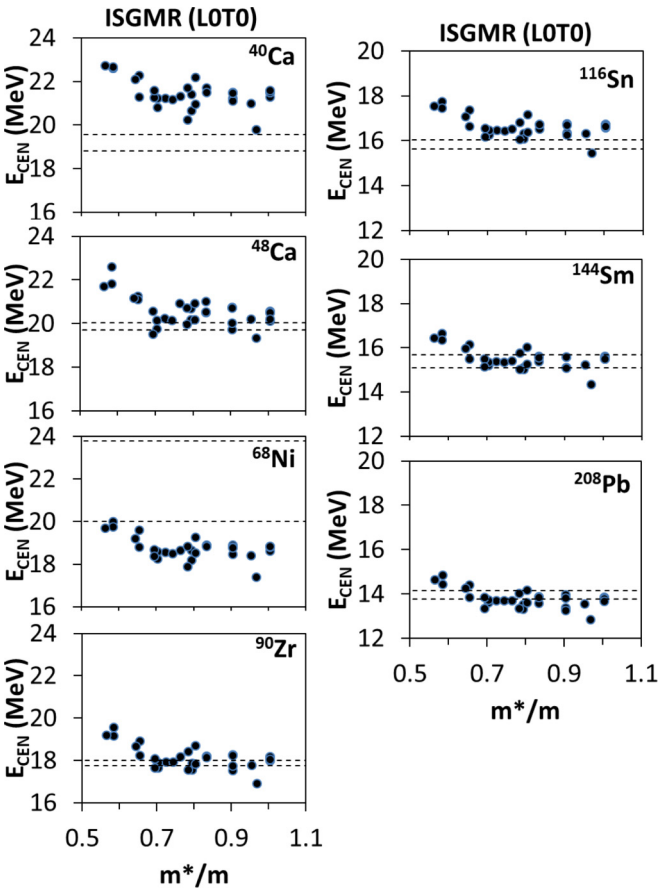


FIG. 3. Similar to Fig. 2, for the effective mass  $m^*/m$ . We find a weak correlation between the calculated values of  $E_{\text{CEN}}$  and  $m^*/m$ , with a Pearson linear correlation coefficient  $C \sim -0.51$ .

of each pair of properties of NM and present the results in Table V. The sensitivity of the centroid energies,  $E_{\text{CEN}}$ , of the giant resonances to NM properties is also investigated by calculating the Pearson linear correlation coefficient  $C$  between the calculated  $E_{\text{CEN}}$ , of each giant resonance, and each property of NM (see Table VI). By comparing the calculated values of  $E_{\text{CEN}}$  to the experimental data we extract constraints on values of NM properties, associated with the standard form of Eq. (1) adopted in this investigation. Considering the limited number of 33 interactions used in this work, we adopt the following nomenclature for the different degrees of correlation: strong ( $|C| > 0.80$ ), medium ( $|C| = 0.61-0.80$ ), weak ( $|C| = 0.35-0.60$ ), and no correlation ( $|C| < 0.35$ ). As seen from Table V, we find no correlations between the values of the NM properties, except for the weak correlations between the values of the effective mass  $m^*/m$  and  $K_{\text{NM}}$  and the medium correlation between  $m^*/m$  and the enhancement coefficient  $\kappa$  for the energy weighted sum rule (EWSR) of the IVGDR, and from weak to strong correlations between symmetry energy coefficients,  $J$ , and its first and second derivatives  $L$  and  $K_{\text{sym}}$ , respectively. These correlations mainly reflect the limited form of the standard

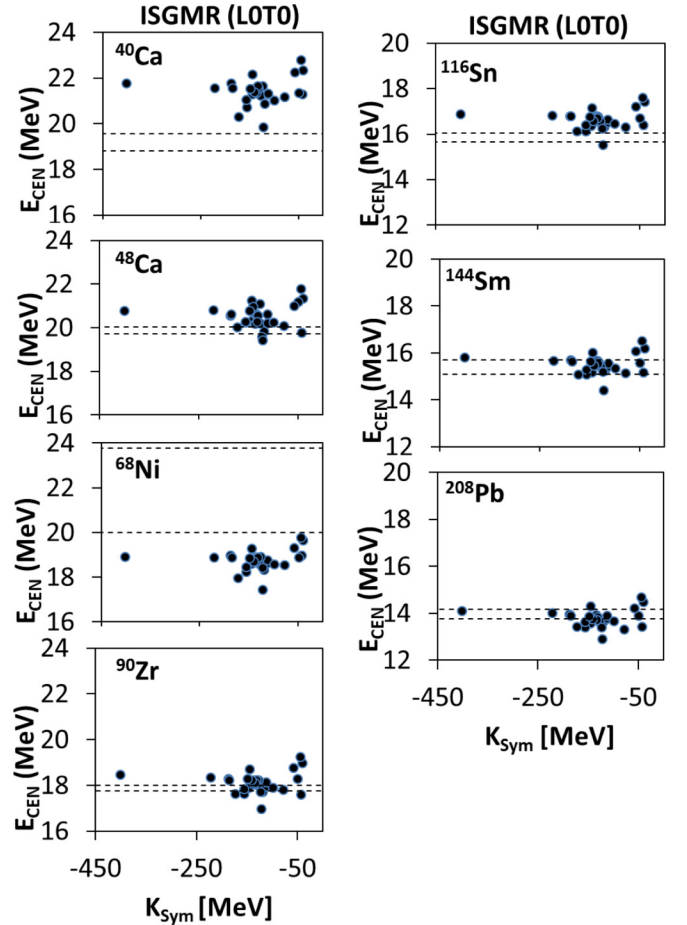


FIG. 4. Similar to Fig. 2 as a function of the second derivative of the symmetry energy coefficient  $K_{\text{sym}}$ . We find weak correlation between the calculated values of  $E_{\text{CEN}}$  and  $K_{\text{sym}}$  with a Pearson linear correlation coefficient  $C \sim 0.45$ .

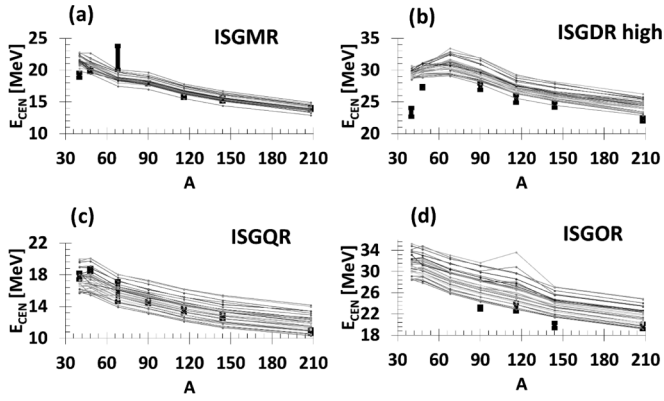


FIG. 5. The centroid energies [MeV] are plotted against the mass  $A$  of each nucleus. Each panel is a different isoscalar multipolarity, (a)  $L = 0$ , (b)  $L = 1$ , (c)  $L = 2$ , and (d)  $L = 3$ . The experimental error bars are shown by the solid vertical lines and are available for all nuclei in  $L = 0$  and  $L = 2$ , for all but  $^{68}\text{Ni}$  in  $L = 1$ , and only for the heavier nuclei,  $^{90}\text{Zr}$ ,  $^{116}\text{Sn}$ ,  $^{144}\text{Sm}$ , and  $^{208}\text{Pb}$  for  $L = 3$ . The theoretical calculations are shown as dots and are connected by lines meant to guide the eye.

Skyrme interaction given in Eq. (1) and may induce spurious correlations, such as the correlation between  $E_{\text{CEN}}$  and  $K_{\text{NM}}$  for isoscalar quadrupole and octupole giant resonances seen

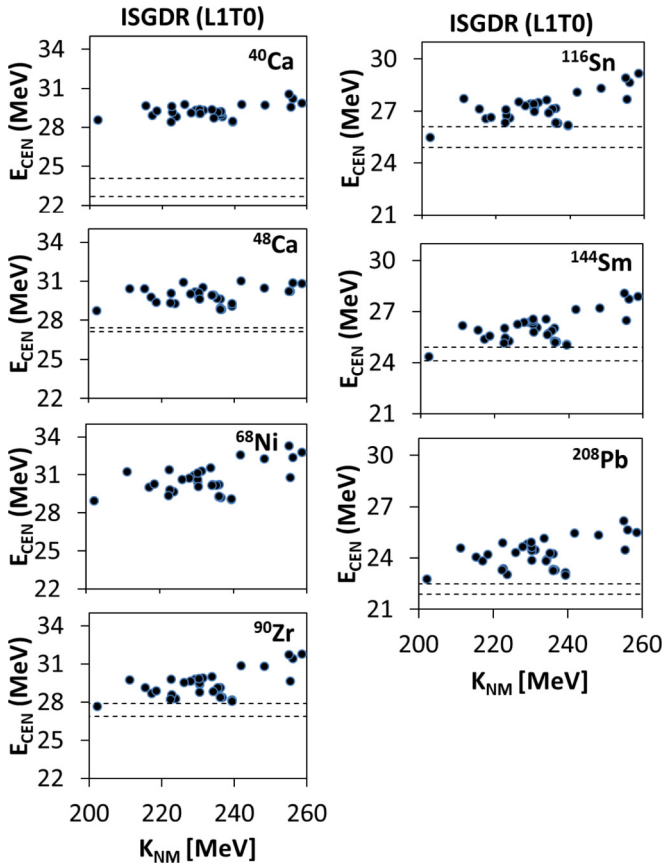


FIG. 6. Similar to Fig. 2, for the isoscalar giant dipole resonance (ISGDR) as a function of  $K_{\text{NM}}$ . We find a weak correlation between the calculated values of  $K_{\text{NM}}$  and  $E_{\text{CEN}}$  with a Pearson linear correlation coefficient  $C \sim 0.52$ .

in Table VI. The spurious correlations can be removed by adopting an extended form of the Skyrme interaction, as done, for example, in Ref. [41]. Other forms of extended Skyrme-type interaction can be found in Ref. [17]. We point out that adopting an extended form for the Skyrme interaction may result with different constraints on the values of NM and nuclear properties see also Refs. [42,43].

In this work we compare the calculated centroid energies  $E_{\text{CEN}}$  with the experimental data, shown in Table VII, with the corresponding experimental errors. The  $^{68}\text{Ni}$  measurement was made at GANIL with inelastic alpha and deuteron scattering at 50A MeV [44]. All the other isoscalar giant resonance data for the centroid energies,  $E_{\text{CEN}}$ , is from the D. H. Youngblood group at Texas A&M University, measured with inelastic scattering of 240 MeV alpha particles [45–48]. A thorough description of the experimental setup can be found in Refs. [49–51]. For the isovector giant resonances monochromatic photon beams were used to measure the photonuclear cross sections [22,52–59], except for the  $^{208}\text{Pb}$  IVGDR, which was done with polarized proton inelastic scattering [60].

In the following sections, we consider each giant resonance separately and present a plot of the corresponding centroid energies, calculated with the HF-RPA method described above for the 33 Skyrme interactions, as a function of a certain nuclear matter property of the corresponding Skyrme

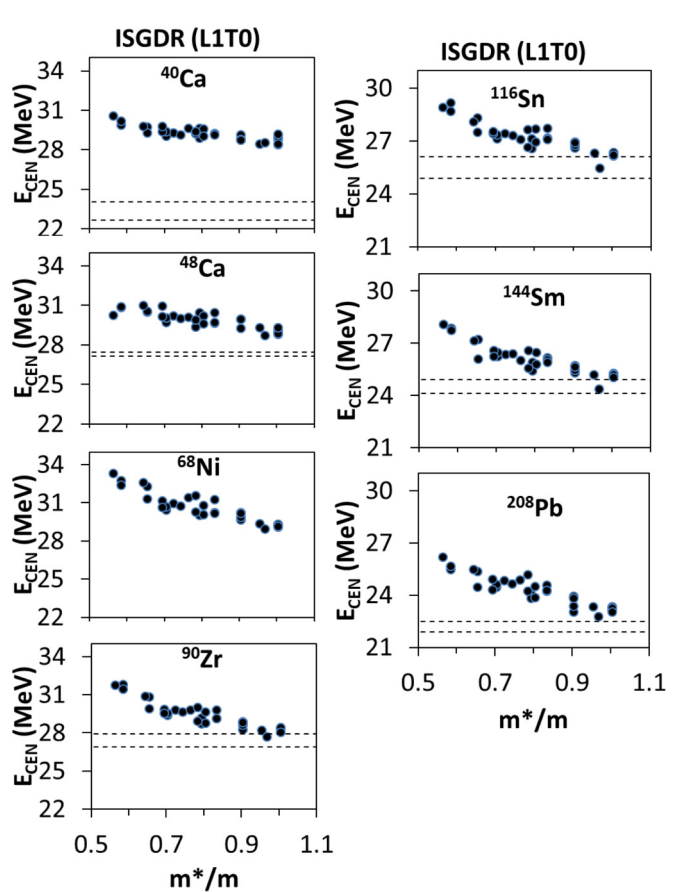


FIG. 7. Similar to Fig. 2, for the ISGDR as a function of  $m^*/m$ . We find strong correlation between the calculated values of  $E_{\text{CEN}}$  and  $m^*/m$  with a Pearson linear correlation coefficient  $C = -0.88$ .



interaction used in the calculation, for the nuclei  $^{40,48}\text{Ca}$ ,  $^{68}\text{Ni}$ ,  $^{90}\text{Zr}$ ,  $^{116}\text{Sn}$ ,  $^{144}\text{Sm}$ , and  $^{208}\text{Pb}$ . When available, experimental data is included in the plots and is delimited by the dashed lines. We also discuss the sensitivities of  $E_{\text{CEN}}$  to bulk properties of nuclear matter.

### A. Isoscalar giant monopole resonance

Figure 2 shows the centroid energy,  $E_{\text{CEN}}$ , of the isoscalar giant monopole resonance (ISGMR) as a function of the nuclear matter incompressibility coefficient  $K_{\text{NM}}$  of the corresponding Skyrme interaction used in the calculation. Each nucleus is plotted separately, and the appropriate experimental band is contained by the dashed lines. Overall we see the well-known strong correlation between the  $E_{\text{CEN}}$  and  $K_{\text{NM}}$  [1,4,61], with a Pearson linear correlation coefficient  $C \sim 0.87$  for all nuclei. We find a weak correlation between  $E_{\text{CEN}}$  and the effective mass  $m^*/m$  with  $C \sim -0.51$ , see Fig. 3. We find that all the interactions considered overestimate the value of  $E_{\text{CEN}}$  of the ISGMR in  $^{40}\text{Ca}$  in disagreement with the experimental data. In  $^{48}\text{Ca}$  some interactions, associated with a value of  $K_{\text{NM}} = 200\text{--}240$  MeV, reproduce the experimental

result for  $E_{\text{CEN}}$ . For the case of  $^{68}\text{Ni}$  we find that all the calculated  $E_{\text{CEN}}$  are a few MeV below the experimental result, except for interactions with very high values ( $\sim 260$  MeV) of  $K_{\text{NM}}$ . On the other hand, for the case of the  $E_{\text{CEN}}$  of  $^{90}\text{Zr}$ ,  $^{144}\text{Sm}$ , and  $^{208}\text{Pb}$  we find that, of the 33 Skyrme interactions considered here, the interactions associated with a value of the incompressibility coefficient between 210 and 240 MeV reproduce the experimental data very well. Lastly, for the case of  $^{116}\text{Sn}$ , the calculated values for  $E_{\text{CEN}}$  are mostly larger (1 MeV) than the experimental result, which is an open problem [62]. We study the centroid energy of the ISGMR as a function of the symmetry energy  $J$  and its first derivative  $L$  and do not find any correlation with the calculated  $E_{\text{CEN}}$  (Pearson linear correlation coefficients  $C = -0.10$  and  $0.25$ , respectively). We point out that we find a weak correlation between the calculated  $E_{\text{CEN}}$  and the second derivative,  $K_{\text{sym}}$ , of the symmetry energy ( $C \sim 0.45$ ), as seen in Fig. 4. We do not find any correlation with any of the other NM properties or with  $W_0$ , see Table VI.

In Fig. 5(a) we plot  $E_{\text{CEN}}$  of the ISGMR for the seven nuclei studied here as a function of their mass,  $A$ . The experimental data and relative error bars, available for all the nuclei studied, are shown by the solid vertical lines, while

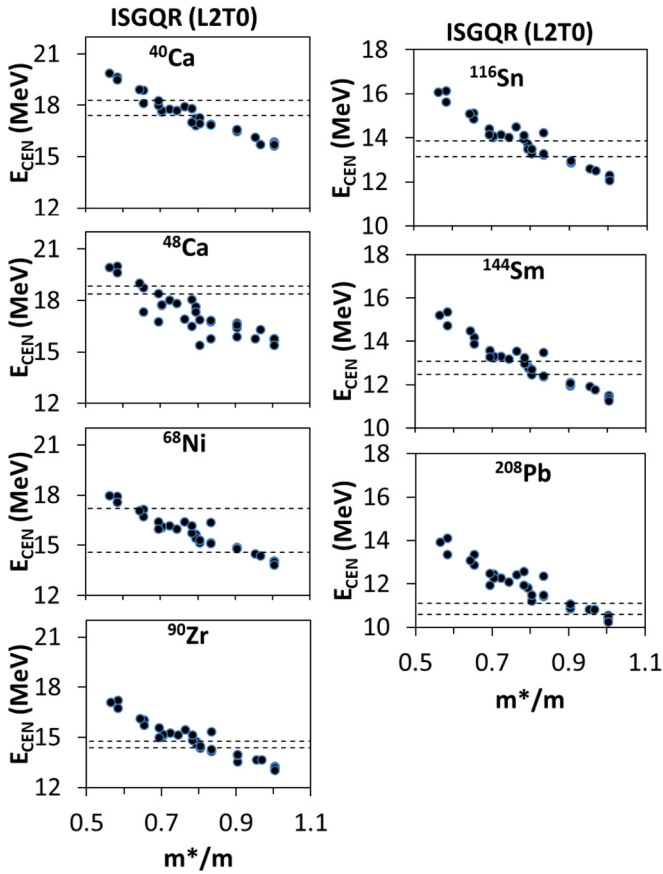


FIG. 8. Similar to Fig. 2, for the isoscalar giant quadrupole resonance (ISGQR) as a function of the effective mass  $m^*/m$ . We find strong correlation between the calculated values of  $m^*/m$  and  $E_{\text{CEN}}$  with a Pearson linear correlation coefficient  $C$  close to  $-0.93$  in all cases.

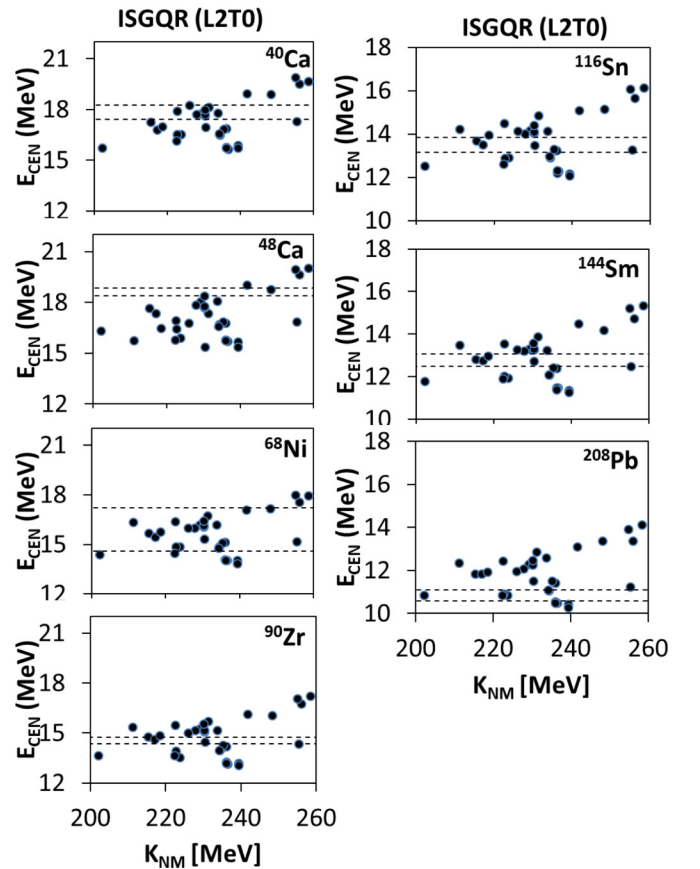


FIG. 9. Similar to Fig. 2, for the ISGQR as a function of the incompressibility coefficient. We find a weak correlation between the calculated values of  $K_{\text{NM}}$  and  $E_{\text{CEN}}$  with a Pearson linear correlation coefficient close to  $C = 0.41$  for all isotopes.

the dots (connected by lines meant to guide the eye) are the theoretical calculations. For the experimental data we find that the value of the centroid energy increases as the mass increases from  $^{40}\text{Ca}$  to  $^{48}\text{Ca}$  to  $^{68}\text{Ni}$ , then starting with  $^{90}\text{Zr}$  we find a decreasing trend. The theory does not reproduce the trend of the lighter nuclei but shows the value of the calculated  $E_{\text{CEN}}$  to steadily decrease as the mass is increased.

### B. Isoscalar giant dipole resonance

The isoscalar dipole response function,  $S(E)$ , is split into low-energy ( $1\hbar\omega$ , excitations) and high-energy ( $3\hbar\omega$ , excitations) components [63–65]. Here we only study the latter, the isoscalar giant dipole resonance (ISGDR). The calculated centroid energies,  $E_{\text{CEN}}$ , (full circles) of the ISGDR are plotted against the NM incompressibility coefficient in Fig. 6. The experimental region is delimited by the dashed lines. We find a weak correlation between  $K_{\text{NM}}$  and the centroid energy (Pearson linear correlation coefficient  $C \sim 0.52$ ). In Fig. 7 we plot the ISGDR centroid energy against the effective mass  $m^*/m$ . We find a strong correlation between  $E_{\text{CEN}}$  and the effective mass with Pearson linear correlation coefficient of  $C \sim -0.88$ . From the figure we see that most of the interactions predict a higher value for the centroid

energy of the ISGDR than the corresponding experimental value. For the two isotopes of  $^{40,48}\text{Ca}$  all the calculated  $E_{\text{CEN}}$  are above the experimental data by up to 6 MeV in some cases. For  $^{90}\text{Zr}$  most interactions are within 2 MeV of the experimental  $E_{\text{CEN}}$ . For  $^{116}\text{Sn}$ ,  $^{144}\text{Sm}$ , and  $^{208}\text{Pb}$  only the interactions with a high value of  $m^*/m$  (i.e., 0.9 and above) reproduce the experimental result. However, we must point out that a comparison between theoretical and experimental results may be misleading since the fraction of the EWSR are quite far from 100% for the Ca isotopes [45,46] but closer to 100% for the heavier nuclei  $^{116}\text{Sn}$ ,  $^{144}\text{Sm}$ , and  $^{208}\text{Pb}$  [48]. These discrepancies between theory and experiment were also pointed out for  $^{40,48}\text{Ca}$  in Ref. [66] and for  $^{116}\text{Sn}$ ,  $^{144}\text{Sm}$ , and  $^{208}\text{Pb}$  in Ref. [48], albeit for a smaller number of interactions. In the case of the symmetry energy terms  $J$  and  $L$ , we do not find any correlation with the calculated centroid energy (Pearson linear correlation coefficients  $C = -0.10$  and  $0.13$ , respectively). For  $K_{\text{sym}}$  we find a weak correlation ( $C = 0.36$ ), similar to the case of the ISGMR. We note that we also find a weak correlation between the calculated values of  $E_{\text{CEN}}$  and the enhancement coefficient,  $\kappa$ , of the EWSR for the IVGDR (Pearson linear correlation coefficient  $C = 0.55$ ), a reflection of the medium correlation between  $\kappa$  and  $m^*/m$

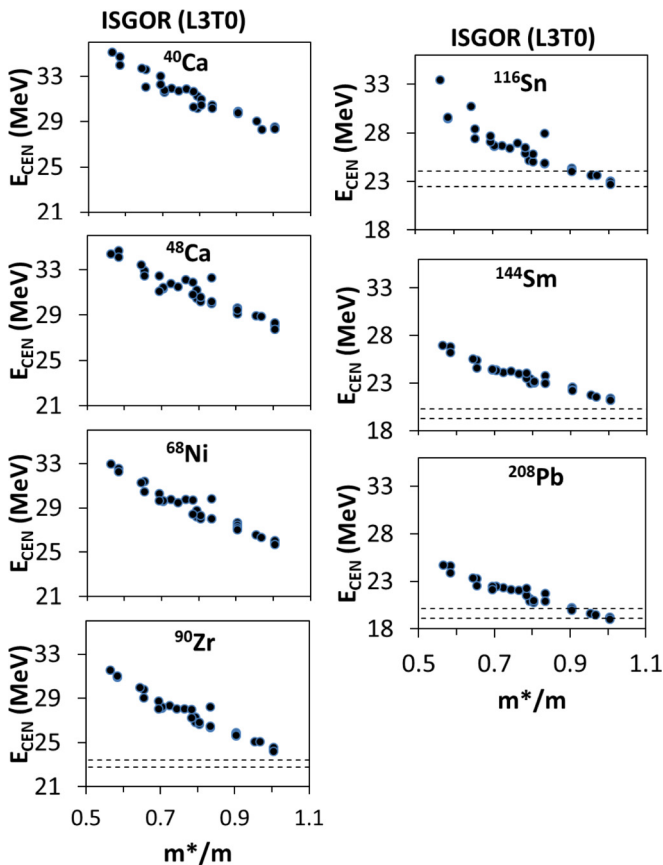


FIG. 10. Similar to Fig. 2, for the isoscalar giant octupole resonance (ISGOR) as a function of the effective mass  $m^*/m$ . We find strong correlation between the calculated values of  $m^*/m$  and  $E_{\text{CEN}}$  with a Pearson linear correlation coefficient  $C = -0.96$  in all cases.

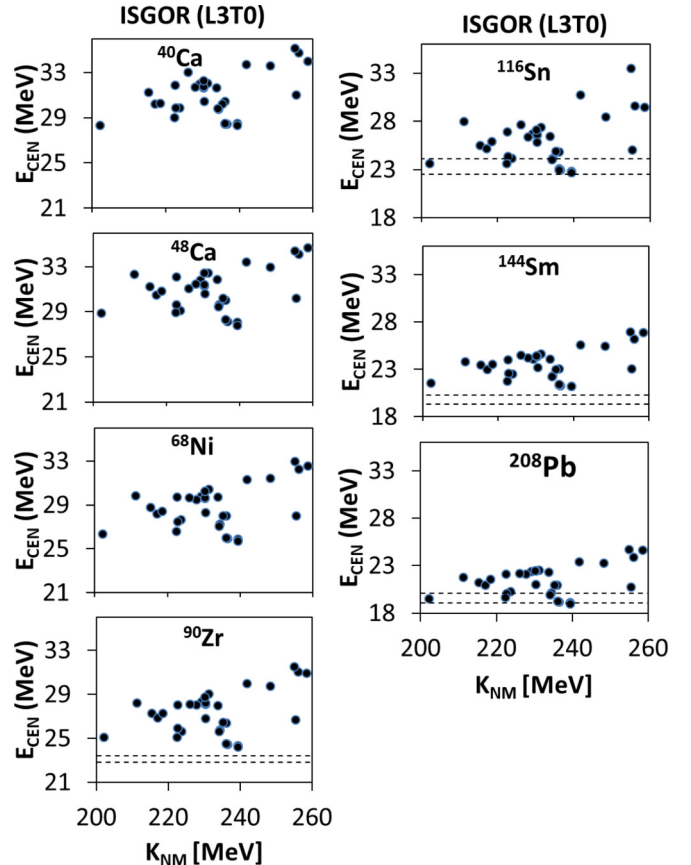


FIG. 11. Similar to Fig. 2, for the ISGOR as a function of the incompressibility coefficient  $K_{\text{NM}}$ . We find a weak correlation between the calculated values of  $K_{\text{NM}}$  and  $E_{\text{CEN}}$  with a Pearson linear correlation coefficient  $C = 0.42$ .

since both are sensitive to the momentum dependent term of the Skyrme interaction, see Tables V and VI.

The calculated values of  $E_{\text{CEN}}$  for the ISGDR are plotted in Fig. 5(b) as a function of mass for the seven nuclei studied here. The experimental region is represented by the solid vertical lines and is available for all but the  $^{68}\text{Ni}$  nucleus. The results of the theoretical calculations are shown as dots connected by lines to guide the eye. As shown in the figure we find that for most interactions, the calculated value of the centroid energy of the ISGDR increases with  $A$  for the lower mass nuclei up to maxima around  $^{68}\text{Ni}$  and decreases later with increasing  $A$ . Similar behavior is seen for the available experimental data.

### C. Isoscalar giant quadrupole resonance

In Fig. 8 we plot the calculated centroid energies,  $E_{\text{CEN}}$ , (full circles) of the isoscalar giant quadrupole resonance (ISGQR) as a function of the effective mass  $m^*/m$  of the corresponding interaction used in the calculation. Each nucleus is plotted separately, and the appropriate experimental band is contained by the dashed lines. We report a decreasing value of  $E_{\text{CEN}}$  as  $m^*/m$  is increased, as well as a strong correlation

between  $E_{\text{CEN}}$  and  $m^*/m$  (Pearson correlation coefficient  $C = -0.93$ ), see also Ref. [66]. In particular, we find that the experimental value of  $E_{\text{CEN}}$  for  $^{40,48}\text{Ca}$ ,  $^{68}\text{Ni}$ ,  $^{90}\text{Zr}$ ,  $^{116}\text{Sn}$ , and  $^{144}\text{Sm}$  agrees with interactions associated with a value of  $m^*/m$  between 0.70–0.90, while for  $^{208}\text{Pb}$  we see that the interactions with an effective mass in the range of 0.8–1.0 best reproduce the experimental result. We find a weak correlation between  $E_{\text{CEN}}$  and  $K_{\text{NM}}$ , with a Pearson linear correlation coefficient  $C = 0.41$ , see Fig. 9. We do not find any correlation between  $E_{\text{CEN}}$  and the symmetry energy terms,  $J$  or  $L$  with Pearson linear correlation coefficients  $C = -0.09$  and 0.15, respectively. However, we find a weak correlation between  $E_{\text{CEN}}$  and  $K_{\text{sym}}$  ( $C = 0.41$ ). We also find a weak correlation between the value of  $E_{\text{CEN}}$  and the enhancement coefficient,  $\kappa$ , of the EWSR for the IVGDR (Pearson linear correlation coefficient  $C = 0.54$ ), a reflection of the medium correlation between  $\kappa$  and  $m^*/m$ , see Tables V and VI.

In Fig. 5(c) we plot  $E_{\text{CEN}}$  of the ISGQR for all the nuclei studied here as a function of the mass of the nucleus,  $A$ . The experimental data and relative error bars are shown by the solid vertical lines, while the dots (connected by lines meant to guide the eye) are the theoretical calculations. We point out a general trend for most of the 33 interactions used here and

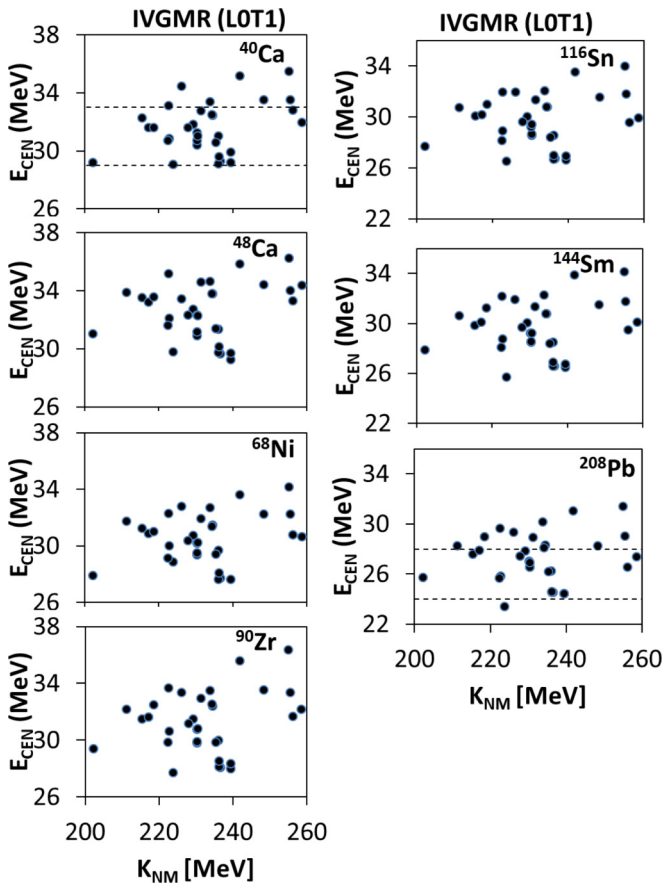


FIG. 12. Similar to Fig. 2, for the isovector giant monopole resonance (IVGMR) as a function of the incompressibility coefficient. We do not find any correlation between the calculated values of  $E_{\text{CEN}}$  and  $K_{\text{NM}}$  with a Pearson linear correlation coefficient  $C = 0.23$  in most cases.

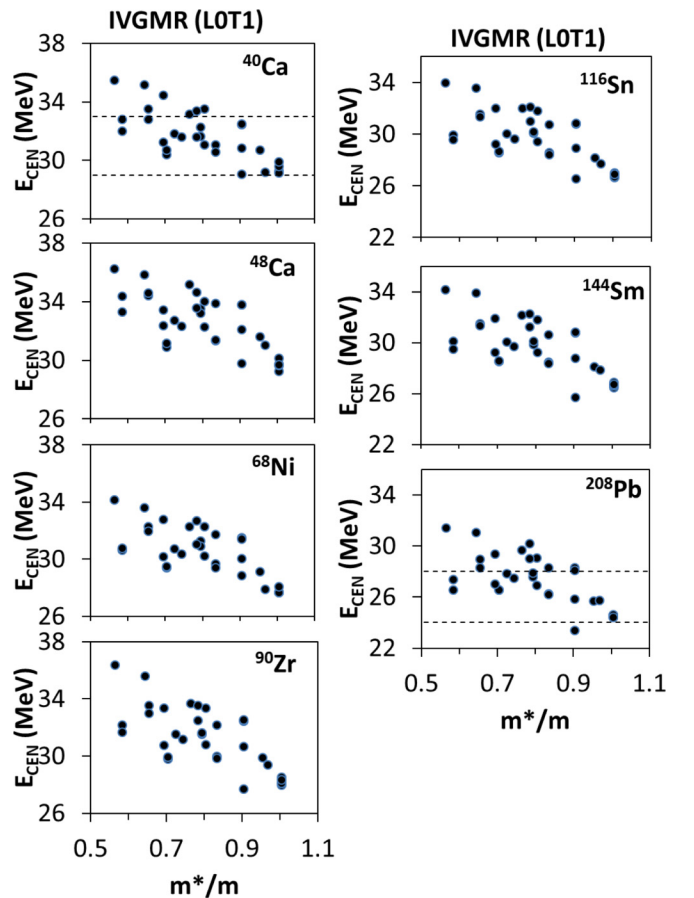


FIG. 13. Similar to Fig. 2, for the IVGMR as a function of the effective mass. We find medium correlation between the calculated values of  $E_{\text{CEN}}$  and  $m^*/m$  with a Pearson linear correlation coefficient  $C = -0.70$ .

the experimental results, predicting a decreasing value of the  $E_{\text{CEN}}$  as  $A$  increases. A notable exception to this is found in  $^{48}\text{Ca}$  whose centroid energy was measured to be higher than that of the lighter isotope  $^{40}\text{Ca}$  by  $0.74 \pm 0.50$  MeV. This trend is reproduced by 17 of the interactions considered, with a difference between the  $E_{\text{CEN}}$  for these two isotopes of up to 0.58 MeV.

#### D. Isoscalar giant octupole resonance

Figure 10 compares the calculated centroid energies,  $E_{\text{CEN}}$ , (full circles) of the isoscalar giant octupole resonance (ISGOR), with the effective mass  $m^*/m$ . The region between the dashed lines is the experimental measurement, available in this case only for the four heaviest nuclei, and each isotope has its own panel. We see a strong correlation between the value of the effective mass and the value of the calculated centroid energy (Pearson linear correlation coefficient  $C \sim -0.96$ ). From the figure we see that the values of  $E_{\text{CEN}}$ , for all the Skyrme parameterizations used in our calculations, are well above the data of  $^{90}\text{Zr}$  and  $^{144}\text{Sm}$ ; however, for  $^{116}\text{Sn}$  and  $^{208}\text{Pb}$  we find that for the interactions with very high effective

mass (above 0.9) the calculated values of  $E_{\text{CEN}}$  are within the experimental error bars. In Fig. 11 we show  $E_{\text{CEN}}$  as a function of the nuclear matter incompressibility  $K_{\text{NM}}$ . We find a weak correlation ( $C = 0.42$ ) between  $E_{\text{CEN}}$  and  $K_{\text{NM}}$ . We do not find any correlation between  $E_{\text{CEN}}$  and the symmetry energy terms,  $J$  or  $L$  with Pearson linear correlation coefficients  $C = -0.10$  and  $0.15$ , respectively. However, we find a weak correlation between  $E_{\text{CEN}}$  and  $K_{\text{sym}}$  ( $C = 0.43$ ), similar to the other isoscalar resonances. We also find a weak correlation between the values of  $E_{\text{CEN}}$  and the enhancement coefficient,  $\kappa$ , of the EWSR for the IVGDR (Pearson linear correlation coefficient  $C = 0.56$ ), a reflection of the medium correlation between  $\kappa$  and  $m^*/m$ , see Tables V and VI.

We summarize in Fig. 5(d) the centroid energies,  $E_{\text{CEN}}$ , of the ISGOR for all the nuclei considered here as a function of their mass,  $A$ . Experimental data is available for the heaviest nuclei  $^{90}\text{Zr}$ ,  $^{116}\text{Sn}$ ,  $^{144}\text{Sm}$ , and  $^{208}\text{Pb}$  and is plotted as solid vertical lines. The dots, connected by lines meant to guide the eye, represent the calculated values of  $E_{\text{CEN}}$ . We find the expected decrease in the value of  $E_{\text{CEN}}$  as  $A$  is increased. However, nine of the interactions considered here predict the value of the centroid energy of  $^{48}\text{Ca}$  above that of  $^{40}\text{Ca}$ . On

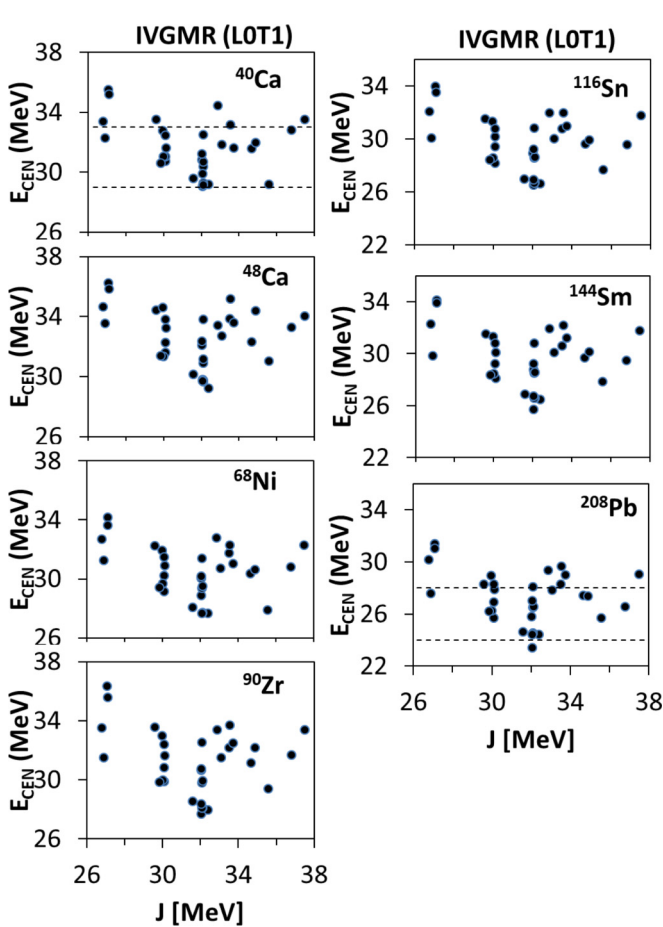


FIG. 14. Similar to Fig. 2, for the IVGMR as a function of the symmetry energy at saturation density,  $J$ . We don't find any correlation between the calculated values of  $J$  and  $E_{\text{CEN}}$  with a Pearson linear correlation coefficient  $C \sim -0.26$ .

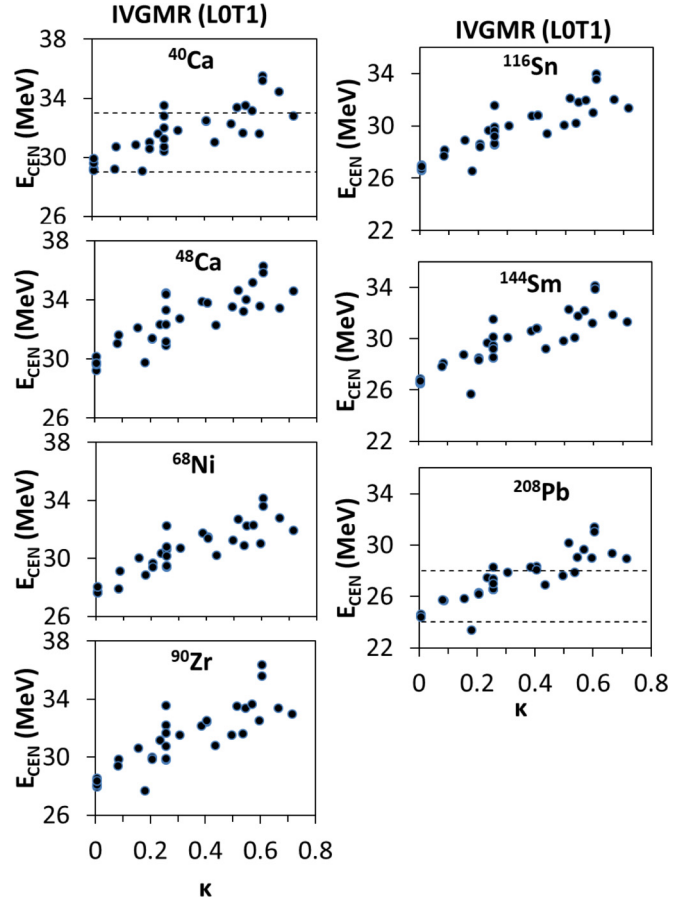


FIG. 15. Similar to Fig. 2, for the IVGMR as a function of the enhancement coefficient,  $\kappa$ , of the EWSR of the IVGDR. We find strong correlation between the calculated values of  $\kappa$  and  $E_{\text{CEN}}$  with a Pearson linear correlation coefficient  $C = 0.86$  for all nuclei considered.



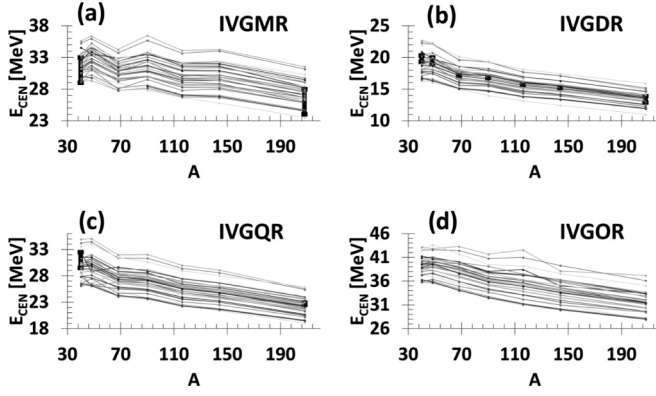


FIG. 16. The centroid energy [MeV] is plotted against the mass  $A$  of each nucleus. Each panel is a different multipolarity, (a)  $L = 0$ , (b)  $L = 1$ , (c)  $L = 2$ , and (d)  $L = 3$ . The experimental error bars are shown by the solid vertical lines and are available only for  $^{40}\text{Ca}$  and  $^{208}\text{Pb}$  in  $L = 0$ , for all nuclei in  $L = 1$ , for  $^{40}\text{Ca}$  and  $^{208}\text{Pb}$  for  $L = 2$  and unavailable for all nuclei for  $L = 3$ . The theoretical calculations are shown as dots and are connected by lines meant to guide the eye.

the other hand, only two interactions predict the value of the centroid energy of  $^{116}\text{Sn}$  above that of  $^{90}\text{Zr}$ , in agreement with available experimental data.

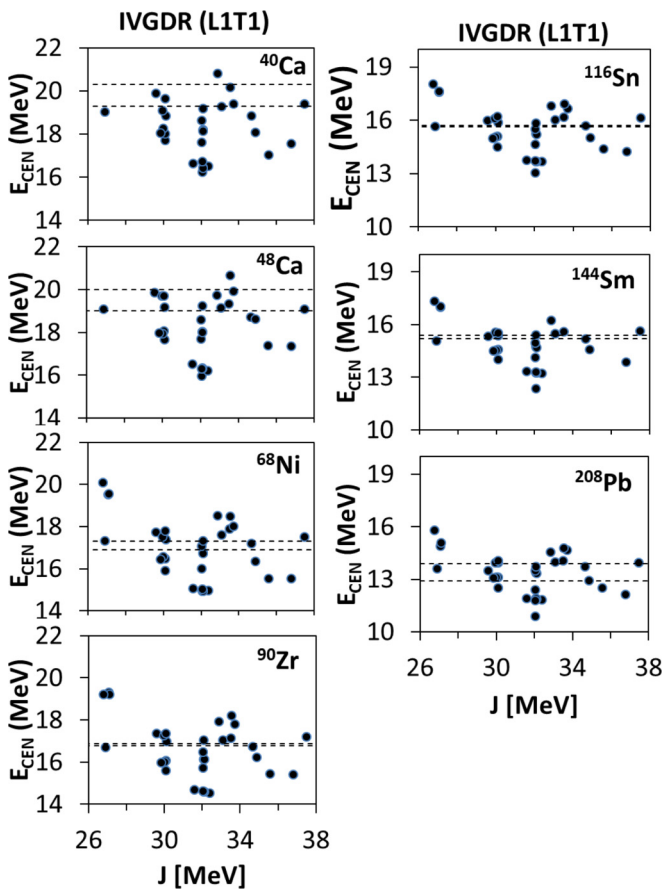


FIG. 17. Similar to Fig. 2, for the isovector giant dipole resonance (IVGDR) as a function of  $J$ . We find a weak correlation between the calculated values of  $J$  and  $E_{\text{CEN}}$  with a Pearson linear correlation coefficient  $C \sim -0.37$ .

### E. Isovector giant monopole resonance

In Fig. 12 we plot the calculated centroid energies,  $E_{\text{CEN}}$ , (full circles) of the isovector giant monopole resonance (IVGMR), an isovector compression mode, as a function of the nuclear matter incompressibility coefficient  $K_{\text{NM}}$ . The experimental result, available for  $^{40}\text{Ca}$  and  $^{208}\text{Pb}$ , is marked by the dashed lines. We do not find any correlation between the values of  $E_{\text{CEN}}$  and  $K_{\text{NM}}$  with a Pearson linear correlation coefficient  $C = 0.23$  for most nuclei. On the other hand, we find a medium correlation between the values of  $E_{\text{CEN}}$  of the IVGMR and  $m^*/m$  (Pearson linear correlation coefficient  $C \sim -0.70$ ) shown in Fig. 13. Next, we consider the isovector NM property of the symmetry energy  $J$  in Fig. 14. We find no correlation between the values of  $E_{\text{CEN}}$  and  $J$  (Pearson linear correlation coefficient  $C \sim -0.26$ ). Similarly, for the first derivative  $L$  and the second derivative  $K_{\text{sym}}$  of  $J$ , we do not find any correlations with the values of the centroid energy (Pearson linear correlation coefficient  $C \sim -0.12$  and  $C \sim 0.00$ , respectively). We find a strong correlation between the values of  $E_{\text{CEN}}$  and the enhancement coefficient,  $\kappa$ , of the EWSR for the IVGDR (Pearson linear correlation coefficient  $C = 0.86$ ) as shown in Fig. 15. However, the experimental

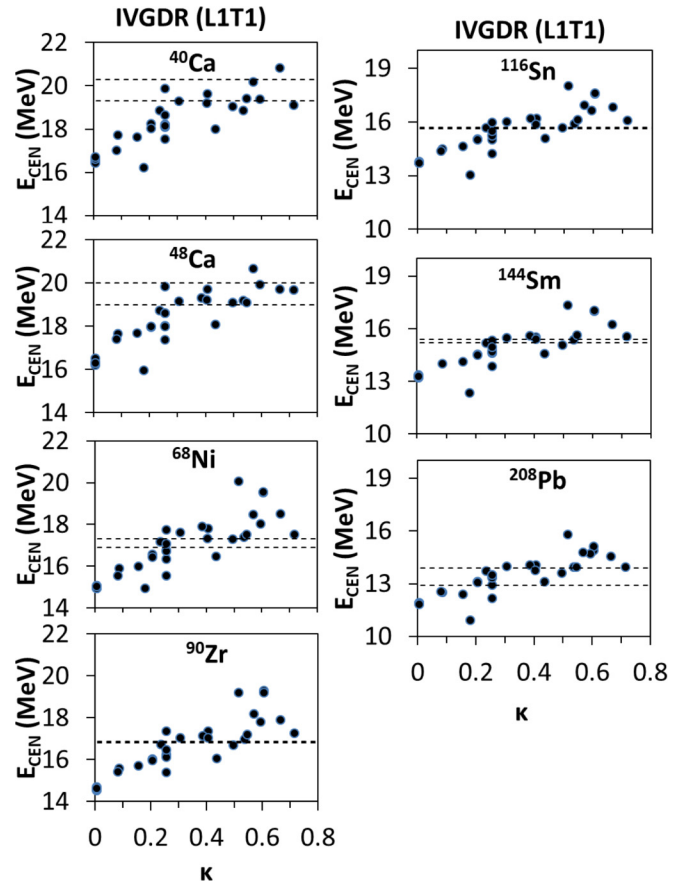


FIG. 18. Similar to Fig. 2, for the IVGDR as a function of the enhancement coefficient,  $\kappa$ , of the EWSR for the IVGDR. We find a strong correlation between the calculated values of  $\kappa$  and  $E_{\text{CEN}}$  with a Pearson linear correlation coefficient  $C = 0.84$  for all nuclei considered.



data for both  $^{40}\text{Ca}$  and  $^{208}\text{Pb}$  has broad error-bars covering most of the interactions considered here and does not allow us to narrow down the value of  $\kappa$  (or any other NM property) using the  $E_{\text{CEN}}$  of the IVGMR.

In Fig. 16(a) we plot the calculated and the available experimental values for  $E_{\text{CEN}}$  of the IVGMR as a function of the mass  $A$ . Most of the 33 interactions used here predict a decreasing see-saw trend in the values of  $E_{\text{CEN}}$  as  $A$  increases. In particular, the calculated values of  $E_{\text{CEN}}$  for  $^{48}\text{Ca}$  are above those of  $^{40}\text{Ca}$  for all but two interactions (NRAPR and SKT3\*). Similarly, the predicted values of  $E_{\text{CEN}}$  for  $^{90}\text{Zr}$  are above those of  $^{68}\text{Ni}$  for all but one interaction (SKO), while the centroid energy of  $^{144}\text{Sm}$  is calculated to be roughly the same as that of  $^{116}\text{Sn}$  (within 0.2 MeV, for most interactions).

### F. Isovector giant dipole resonance

The calculated centroid energies,  $E_{\text{CEN}}$ , of the isovector giant dipole resonance (IVGDR) show a weak correlation with the symmetry energy coefficient  $J$  (Pearson linear correlation coefficient  $C \sim -0.37$ ), as can be seen in Fig. 17. The experimental data for  $E_{\text{CEN}}$  is delimited by the dashed lines. We point out that the experimental errors for  $^{90}\text{Zr}$  and  $^{116}\text{Sn}$  are too small, making them hard to distinguish.

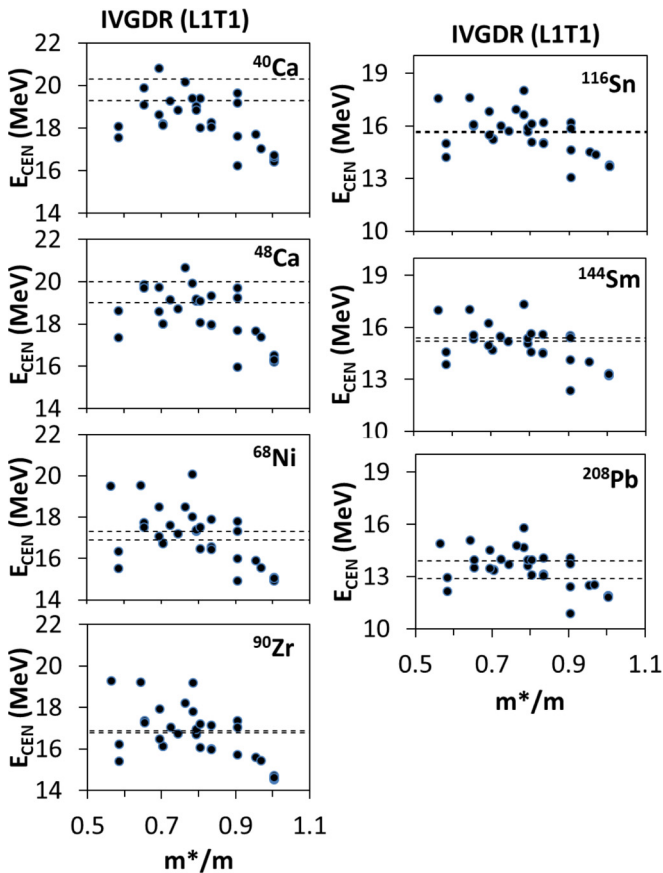


FIG. 19. Similar to Fig. 2, for the IVGDR as a function of the effective mass. We find a weak correlation between the calculated values of  $m^*/m$  and  $E_{\text{CEN}}$  with a Pearson linear correlation coefficient close to  $C = -0.60$  for all the nuclei considered here.

Similar results to those obtained for the correlation between the values of  $E_{\text{CEN}}$  and the symmetry energy are found for its first derivatives,  $L$  (Pearson linear correlation coefficient  $C \sim -0.42$ ) no correlation with its and second derivative  $K_{\text{sym}}$  (Pearson linear correlation coefficient  $C \sim -0.30$ ). It is commonly expected that the value of  $E_{\text{CEN}}$  for the IVGDR is quite sensitive to the density dependence of  $E_{\text{sym}}(\rho)$  [22,67], however, our calculated Pearson linear correlation coefficients do not reflect this. Similar to the results of Ref. [66], we find a strong correlation (Pearson linear correlation coefficient  $C = 0.84$ ) between the calculated values of  $E_{\text{CEN}}$  and the EWSR enhancement coefficient,  $\kappa$ , of the IVGDR, plotted in Fig. 18, especially for the heavier nuclei. We find that the experimental data of  $E_{\text{CEN}}$  for most nuclei agrees with interactions associated with a value of  $\kappa$  between 0.25 and 0.7. In Fig. 19, we show the centroid energy as a function of the effective mass  $m^*/m$ . We find a weak correlation between the values of  $E_{\text{CEN}}$  and  $m^*/m$  with a Pearson linear correlation coefficient close to  $C = -0.60$ , for all the nuclei. As seen from Table VI, we do not find any correlation between  $E_{\text{CEN}}$  and  $K_{\text{NM}}$  ( $C \sim 0.05$ ).

In Fig. 16(b) we plot the calculated and experimental values of  $E_{\text{CEN}}$  of the IVGDR for the seven nuclei studied here

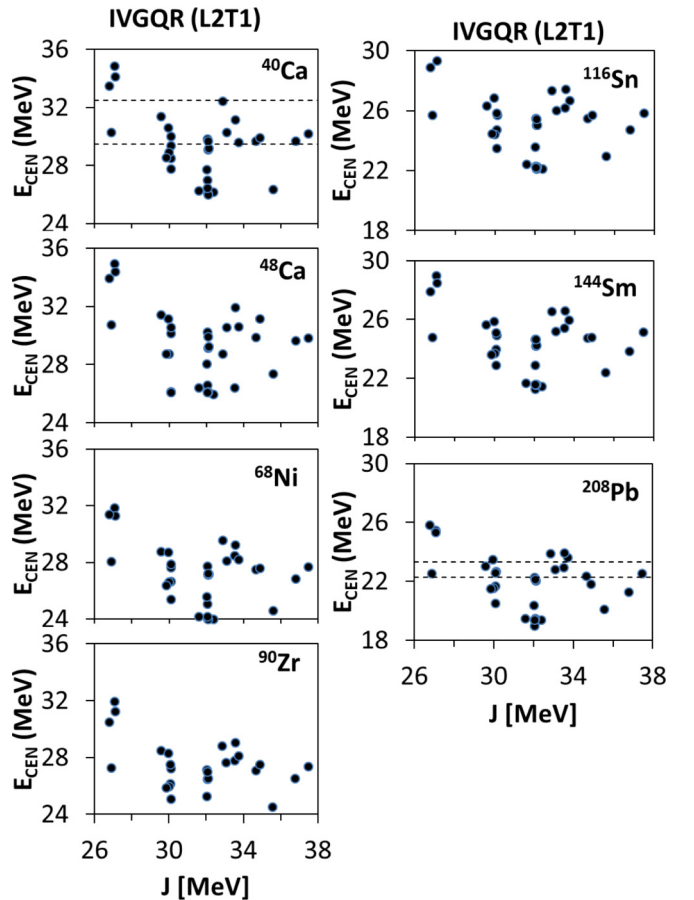


FIG. 20. Similar to Fig. 2, for the isovector giant quadrupole resonance (IVGQR) as a function of the symmetry energy coefficient  $J$ . We find a weak correlation between the calculated values of  $J$  and  $E_{\text{CEN}}$  with a Pearson linear correlation coefficient  $C \sim -0.35$ .

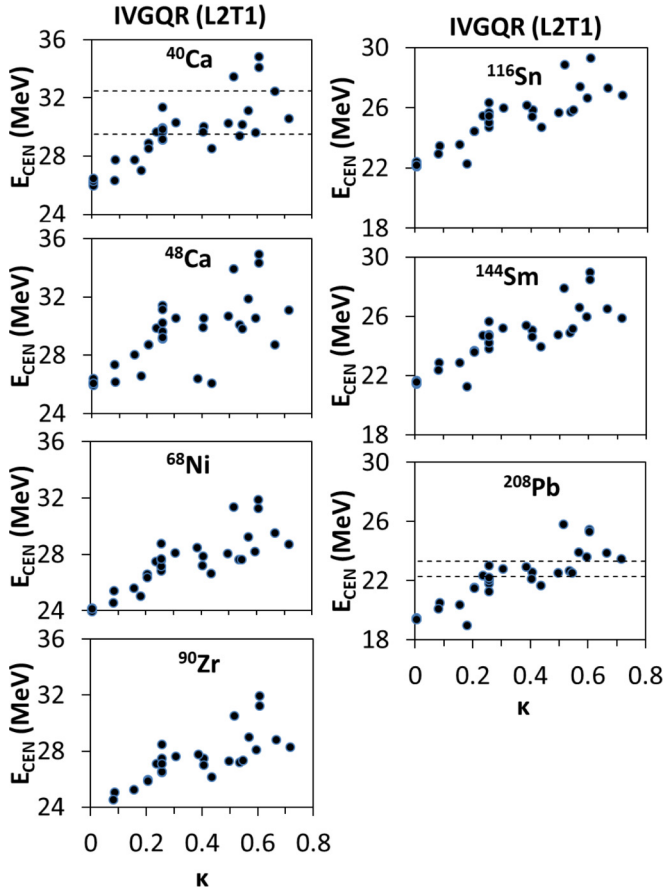


FIG. 21. Similar to Fig. 2, for the IVGQR as a function of the enhancement coefficient,  $\kappa$ , of the EWSR of the IVGDR. We find medium correlation between the calculated values of  $\kappa$  and  $E_{\text{CEN}}$  with a Pearson linear correlation coefficient  $C = 0.80$  for all nuclei considered.

as a function of the mass  $A$ . It is seen from the figure that the experimental values of  $E_{\text{CEN}}$  decrease with  $A$ . Similarly, most of the 33 Skyrme interactions used here predict a decreasing value of the  $E_{\text{CEN}}$  with  $A$ . Deviations to this decreasing trend are found for 12 of the interactions considered, which predict the value of the centroid energy for  $^{48}\text{Ca}$  to be higher, by up to 0.60 MeV, than that of  $^{40}\text{Ca}$ .

### G. Isovector giant quadrupole resonance

In Fig. 20 we show the calculated  $E_{\text{CEN}}$  for the isovector giant quadrupole resonance (IVGQR) as a function of the symmetry energy  $J$ . The experimental data, only available for  $^{40}\text{Ca}$  and  $^{208}\text{Pb}$  in this case, is marked by dashed lines. We find a weak correlation between the calculated values of  $J$  and  $E_{\text{CEN}}$  with a Pearson linear correlation coefficient  $C \sim -0.35$ . We don't find any correlation between the calculated values of the first derivative of the symmetry energy  $L$  and  $E_{\text{CEN}}$  (Pearson linear correlation coefficient  $C \sim -0.29$ ), as well as for the second derivative of the symmetry energy  $K_{\text{sym}}$  and the value of  $E_{\text{CEN}}$  (Pearson linear correlation coefficient  $C \sim -0.13$ ). On the other hand, we find in Fig. 21 a medium correlation ( $C \sim 0.80$ ) between  $E_{\text{CEN}}$  and the EWSR

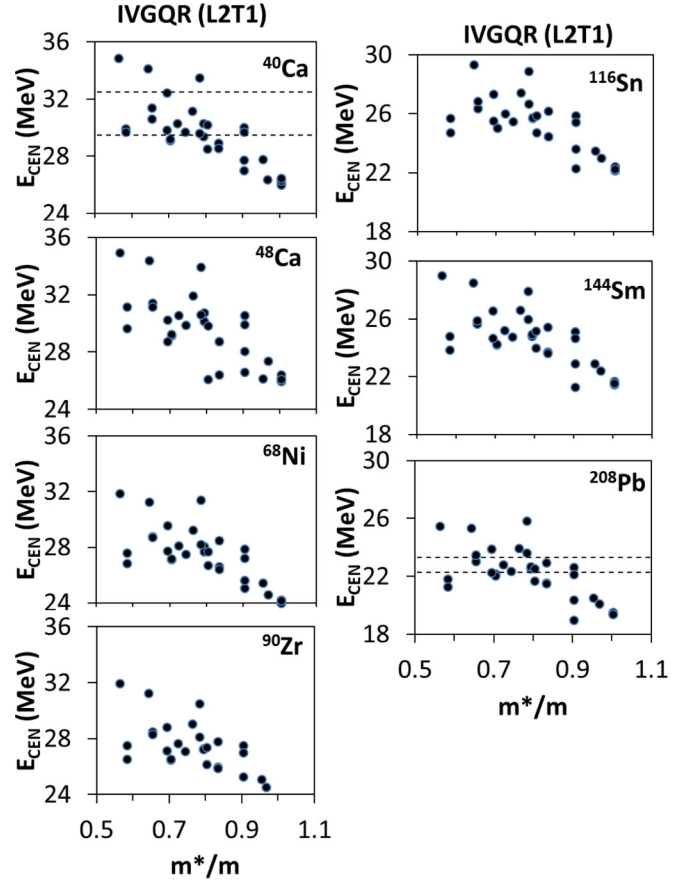


FIG. 22. Similar to Fig. 2, for the IVGQR as a function of the effective mass  $m^*/m$ . We find medium correlation between the calculated values of  $m^*/m$  and  $E_{\text{CEN}}$  with a Pearson linear correlation coefficient of  $C = -0.74$  for all the nuclei considered here.

enhancement coefficient,  $\kappa$ , of the IVGDR. We find that of the 33 interactions we considered here the ones with a value of  $\kappa$  between 0.25 and 0.7 best reproduce the experimental value of  $E_{\text{CEN}}$ , in agreement with our above finding for the case of the IVGDR. In Fig. 22 we demonstrate a medium correlation between the values of  $E_{\text{CEN}}$  and  $m^*/m$  ( $C \sim -0.74$ ), with the interactions that have a value of  $m^*/m$  between 0.6 and 0.9 reproducing the available experimental results the best. As seen from Table VI, we do not find any correlation between the calculated values of  $E_{\text{CEN}}$  and  $K_{\text{NM}}$  ( $C \sim 0.18$ ).

In Fig. 16(c) we plot the  $E_{\text{CEN}}$  of the IVGQR as a function  $A$ . From the theoretical calculations we see a general trend of a decreasing value of  $E_{\text{CEN}}$  as  $A$  increases. In contrast with the general trend, for the case of the Ca isotopes we find that only nine of the interactions considered predict the value of the centroid energy of  $^{48}\text{Ca}$  below that of  $^{40}\text{Ca}$  (but only six interactions do so by more than 0.30 MeV).

### H. Isovector giant octupole resonance

No experimental data is available for the centroid energy of the isovector giant octupole resonance (IVGOR). In Fig. 23 we study the centroid energy,  $E_{\text{CEN}}$ , of the IVGOR, as a function of the symmetry energy  $J$ . We do not find any

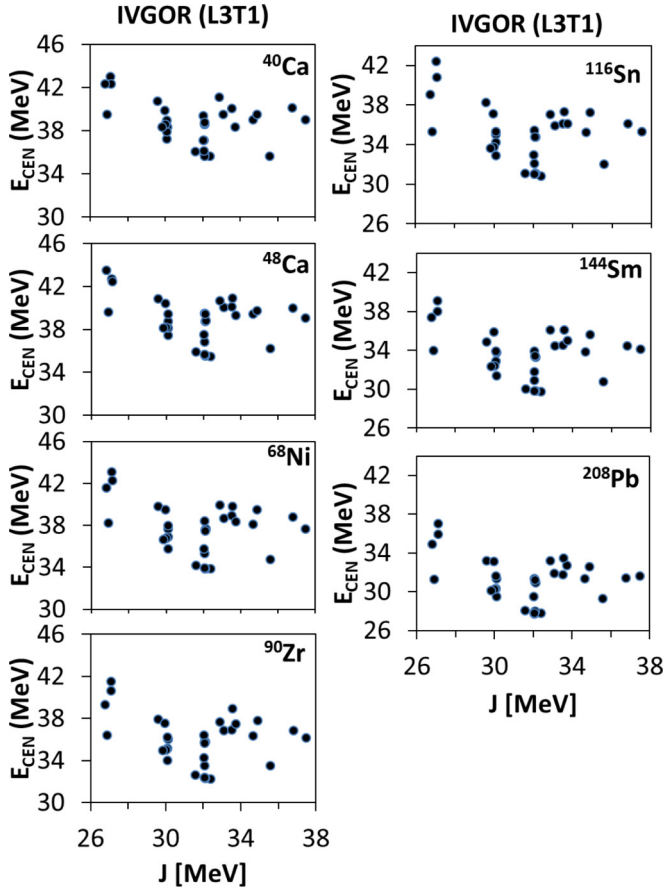


FIG. 23. Similar to Fig. 2, for the isovector giant octupole resonance (IVGOR) as a function of the symmetry energy coefficient  $J$ . We don't find any correlation between the calculated values of  $J$  and  $E_{\text{CEN}}$  with a Pearson linear correlation coefficient  $C \sim -0.32$ .

correlation between the value of the calculated  $E_{\text{CEN}}$  and  $J$ , with a Pearson linear correlation coefficient  $C = -0.32$ . Likewise, for the first and second derivatives of the symmetry energy, we do not find any correlation between the values of  $E_{\text{CEN}}$  and both  $L$  or  $K_{\text{sym}}$  (with Pearson linear correlation coefficients  $C \sim -0.19$  and  $C \sim 0.02$ , respectively). On the other hand, we find a strong correlation between the  $E_{\text{CEN}}$  and the EWSR enhancement coefficient,  $\kappa$ , for the IVGDR (Pearson correlation coefficient  $C \sim 0.81$ ) as can be seen in Fig. 24. Also, for the case of the effective mass  $m^*/m$ , shown in Fig. 25, we report a strong correlation with the value of the centroid energy (Pearson linear correlation coefficient  $C \sim -0.83$ ). As seen from Table VI, we do not find any correlation between the value of  $E_{\text{CEN}}$  and  $K_{\text{NM}}$  ( $C \sim 0.25$ ).

We report a decreasing trend in the calculated value of  $E_{\text{CEN}}$  of the IVGOR as the nucleon mass  $A$  is increased, see Fig. 16(d). We note some exceptions for the calculated value of  $E_{\text{CEN}}$  of  $^{48}\text{Ca}$ , which many (22 of the 33) interactions predict above that of  $^{40}\text{Ca}$ , although not by a significant amount in most cases.

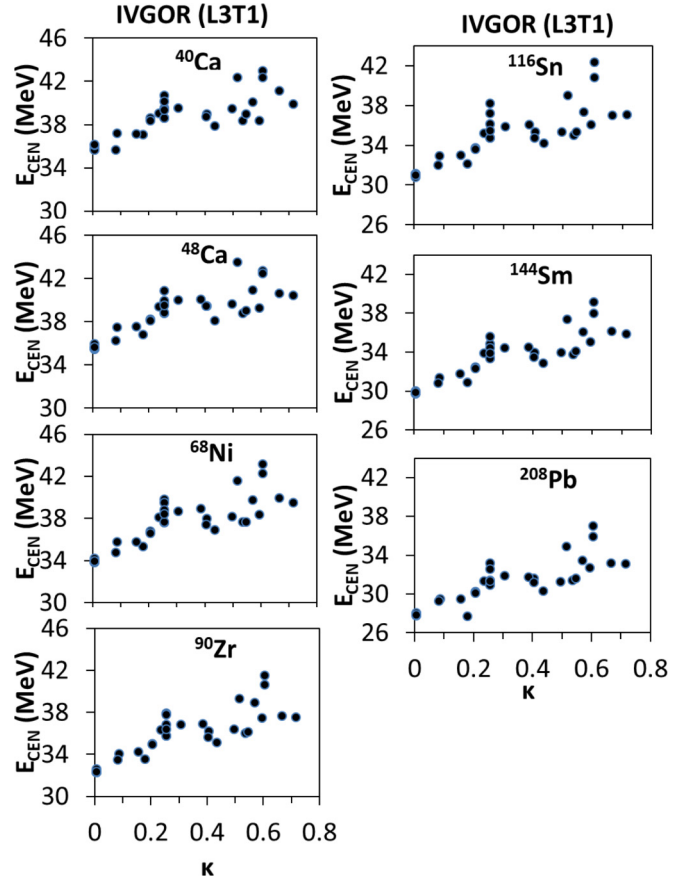


FIG. 24. Similar to Fig. 2, for the IVGOR as a function of the enhancement coefficient,  $\kappa$ , for the EWSR of the ISGDR. We find strong correlation between the calculated values of  $\kappa$  and  $E_{\text{CEN}}$  with a Pearson linear correlation coefficient  $C = 0.81$  for all nuclei considered.

#### IV. SUMMARY AND CONCLUSIONS

In this work we have presented results of fully self-consistent spherical HF-RPA calculations, using the 33 commonly employed Skyrme-type effective nucleon-nucleon interactions of the standard form, Eq. (1), shown in Table I, for the centroid energies,  $E_{\text{CEN}}$ , of the isoscalar and isovector giant resonances of multipolarities  $L = 0-3$  in  $^{40,48}\text{Ca}$ ,  $^{68}\text{Ni}$ ,  $^{90}\text{Zr}$ ,  $^{116}\text{Sn}$ ,  $^{144}\text{Sm}$ , and  $^{208}\text{Pb}$  and compared with available experimental data. For the heavier nuclei,  $^{90}\text{Zr}$ ,  $^{116}\text{Sn}$ ,  $^{144}\text{Sm}$ , and  $^{208}\text{Pb}$ , we obtained good agreement between theory and experiment for the ISGMR, ISGQR, and IVGDR for the calculated values of  $E_{\text{CEN}}$  for some of the 33 Skyrme interactions used in our work. As the mass increases from  $^{40}\text{Ca}$ , to  $^{48}\text{Ca}$  to  $^{68}\text{Ni}$ , we do not see an increasing value of the calculated  $E_{\text{CEN}}$  of the ISGMR, in sharp contrast to the experimental data. All the interactions considered overestimate the  $E_{\text{CEN}}$  of the ISGMR in  $^{40}\text{Ca}$  and underestimate it for  $^{68}\text{Ni}$ . However, the ISGMR centroid energy of  $^{48}\text{Ca}$  is reproduced by many interactions. We point out that for most nuclei the calculated values of  $E_{\text{CEN}}$  of the ISGDR and ISGOR are significantly above (over 1 MeV) the corresponding experimental values.

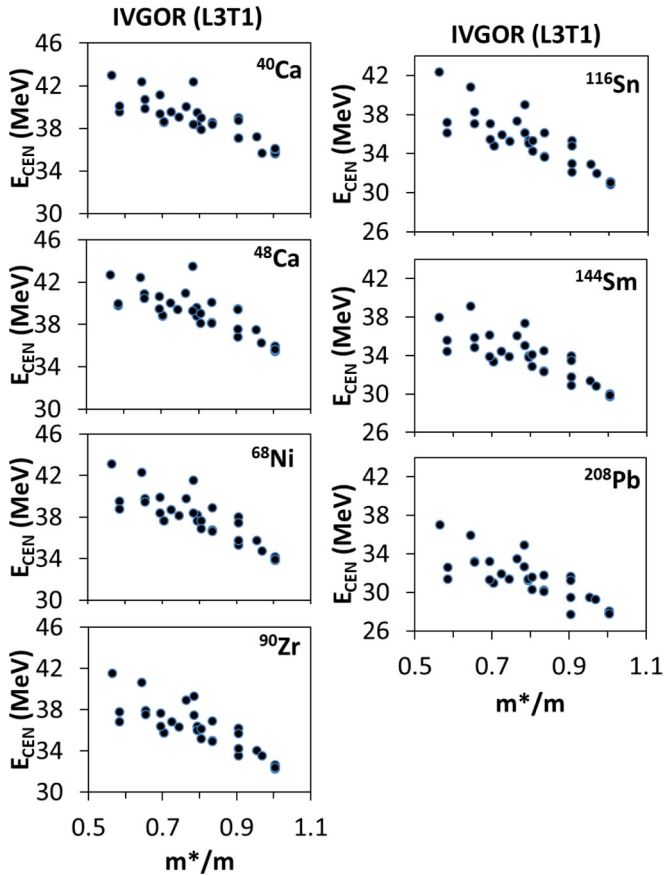


FIG. 25. Similar to Fig. 2, for the calculated values of the IVGOR as a function of the effective mass  $m^*/m$ . We find strong correlation between the calculated values of  $m^*/m$  and  $E_{\text{CEN}}$  with a Pearson linear correlation coefficient  $C = -0.83$  for all nuclei considered.

We also studied the sensitivity of the calculated centroid energies,  $E_{\text{CEN}}$ , of the giant resonances to various properties of nuclear matter at saturation density, associated with the adopted standard form of Eq. (1) of Skyrme-type effective nucleon-nucleon interactions, by determining the corresponding Pearson linear correlation coefficients  $C$ . This allows us to constrain the values of NM properties, associated with this form of interaction. For the correlations between the calculated values of  $E_{\text{CEN}}$  and the nuclear matter incompressibility coefficient  $K_{\text{NM}}$  we find strong, weak, and no correlations for the compression modes of the ISGMR, ISGDR, and the IVGMR, respectively. For the correlations between the calculated values of  $E_{\text{CEN}}$  and the effective mass  $m^*/m$  we find strong correlations for the ISGDR, ISGQR, ISGOR, and IVGOR and medium correlations for the IVGMR, IVGDR, and IVGQR. We also find, for all the isovector giant resonances, strong correlations between the calculated values of  $E_{\text{CEN}}$  and the values of the enhancement coefficient,  $\kappa$ , for the energy weighted sum rule of the isovector giant dipole resonance. It is important to note that we find no correlations between the calculated values of  $E_{\text{CEN}}$  and the symmetry energy coefficient  $J$ , or its first derivative  $L$ , for all the isoscalar giant resonances of multipolarities  $L = 0-3$ . We point out that we find weak

correlations between  $E_{\text{CEN}}$  and  $K_{\text{sym}}$ , the second derivative of  $J$ , for all the isoscalar giant resonances of multipolarities  $L = 0-3$  for the symmetric nucleus  $^{40}\text{Ca}$  as well as for the asymmetric nuclei  $^{48}\text{Ca}$ ,  $^{68}\text{Ni}$ ,  $^{90}\text{Zr}$ ,  $^{116}\text{Sn}$ ,  $^{144}\text{Sm}$ , and  $^{208}\text{Pb}$ . We find no correlations between the calculated values of  $E_{\text{CEN}}$  and  $J$ ,  $L$  or  $K_{\text{sym}}$  for the IVGMR and IVGOR. For the IVGDR we find weak correlations between  $E_{\text{CEN}}$  and both  $J$ , and  $L$  and no correlation with  $K_{\text{sym}}$ . For the IVGQR, we find a weak correlation between  $E_{\text{CEN}}$  and  $J$  and no correlations with  $L$  or  $K_{\text{sym}}$ . To better determine the density dependence of the symmetry energy  $E_{\text{sym}}(\rho)$  one should consider the dependence of  $E_{\text{CEN}}$  on neutron-proton asymmetry,  $(N-Z)/A$ , and other properties such as the IVGDR polarizability, which is the subject of further investigations, see for example Ref. [68].

In summary, considering the calculated HF-based RPA results for the  $E_{\text{CEN}}$  for the ISGMR, ISGQR, and IVGDR of  $^{40,48}\text{Ca}$ ,  $^{68}\text{Ni}$ ,  $^{90}\text{Zr}$ ,  $^{116}\text{Sn}$ ,  $^{144}\text{Sm}$ , and  $^{208}\text{Pb}$  we obtained good agreement with the experimental data for some interactions. Comparing the calculated  $E_{\text{CEN}}$  to the experimental results we find that:

- (i) Strong correlations exist between the calculated centroid energies  $E_{\text{CEN}}$  of the isoscalar giant monopole resonance (ISGMR) and the nuclear matter (NM) incompressibility coefficient,  $K_{\text{NM}}$ , leading to the value of  $K_{\text{NM}} = 210-240$  MeV.
- (ii) Strong correlations exist between the energy of the isovector giant dipole resonance (IVGDR) and the enhancement coefficient  $\kappa$  for the energy weighted sum rule, leading to an accepted value in the range of  $\kappa = 0.25-0.70$ .

We note that these constraints on the values of  $K_{\text{NM}}$  and  $\kappa$  can be used for determining a modern energy density functional (EDF), associated with the standard form of the Skyrme interaction, Eq. (1), adopted in our calculations. This can be done by imposing constraints on the fit and thereby better determine the values of the parameters of Eq. (1), see Ref. [25]. We add that, of course, the constraints on the values of  $K_{\text{NM}}$  and  $\kappa$  may depend on the specific form of the interaction. However, the sensitivity of the centroid energy of the ISGMR to the value of  $K_{\text{NM}}$  was confirmed in previous investigations using various models for the nucleon-nucleon interaction; see for example Ref. [27] for the consistency between relativistic to nonrelativistic models. The value of  $\kappa$  is very sensitive to the EWSR of the IVGDR, which is given by a constant value times  $(1 + \kappa)$ , see Eq. (18). The centroid energy of the ISGQR is sensitive the value of  $m^*/m$ , since  $m^*/m$  affects the spacing between major shell in nuclei and thereby the distribution of the response function. The variation between nuclei for the extracted range of  $m^*/m$ , seen in Fig. 8, may require further experimental and theoretical investigation.

#### ACKNOWLEDGMENT

This work was supported in part by US Department of Energy under Grant No. DE-FG03-93ER40773.



- [1] A. Bohr and B. M. Mottelson, *Nuclear Structure II* (Benjamin, New York, 1975).
- [2] P. Ring and P. Schuck, *The Nuclear Many-Body Problem* (Springer-Verlag, Berlin, 1980).
- [3] M. N. Harakeh and A. van der (Adriaan) Woude, *Giant Resonances : Fundamental High-Frequency Modes of Nuclear Excitation* (Oxford University Press, Oxford, 2001).
- [4] S. Shlomo, V. M. Kolomietz, and G. Colò, *Eur. Phys. J. A* **30**, 23 (2006).
- [5] N. K. Glendenning, *Phys. Rev. C* **37**, 2733 (1988).
- [6] J. M. Lattimer and M. Prakash, *Phys. Rep.* **442**, 109 (2007).
- [7] W. D. Myers and W. J. Świątecki, *Phys. Rev. C* **57**, 3020 (1998).
- [8] L. Satpathy, V. S. U. Maheswari, and R. C. Nayak, *Phys. Rep.* **319**, 85 (1999).
- [9] G. C. Baldwin and G. S. Klaiber, *Phys. Rev.* **71**, 3 (1947).
- [10] M. B. Lewis and F. E. Bertrand, *Nucl. Phys. A* **196**, 337 (1972).
- [11] R. Pitthan and T. Walcher, *Phys. Lett. B* **36**, 563 (1971).
- [12] D. H. Youngblood, C. M. Rozsa, J. M. Moss, D. R. Brown, and J. D. Bronson, *Phys. Rev. Lett.* **39**, 1188 (1977).
- [13] T. H. R. Skyrme, *Philos. Mag.* **1**, 1043 (1956).
- [14] T. H. R. Skyrme, *Nucl. Phys.* **9**, 615 (1958).
- [15] D. Vautherin and D. M. Brink, *Phys. Rev. C* **5**, 626 (1972).
- [16] M. Bender, P.-H. Heenen, and P.-G. Reinhard, *Rev. Mod. Phys.* **75**, 121 (2003).
- [17] M. Dutra, O. Lourenço, J. S. Sá Martins, A. Delfino, J. R. Stone, and P. D. Stevenson, *Phys. Rev. C* **85**, 035201 (2012).
- [18] E. Chabanat, P. Bonche, P. Haensel, J. Meyer, and R. Schaeffer, *Nucl. Phys. A* **627**, 710 (1997).
- [19] T. Sil, S. Shlomo, B. K. Agrawal, and P.-G. Reinhard, *Phys. Rev. C* **73**, 034316 (2006).
- [20] S. Shlomo and A. I. Sanzhur, *Phys. Rev. C* **65**, 044310 (2002).
- [21] B. K. Agrawal, S. Shlomo, and A. I. Sanzhur, *Phys. Rev. C* **67**, 034314 (2003).
- [22] E. Lipparini and S. Stringari, *Phys. Rep.* **175**, 103 (1989).
- [23] B. K. Agrawal and S. Shlomo, *Phys. Rev. C* **70**, 014308 (2004).
- [24] N. Van Giai and H. Sagawa, *Phys. Lett. B* **106**, 379 (1981).
- [25] B. K. Agrawal, S. Shlomo, and V. K. Au, *Phys. Rev. C* **72**, 014310 (2005).
- [26] J. Bartel, P. Quentin, M. Brack, C. Guet, and H.-B. Håkansson, *Nucl. Phys. A* **386**, 79 (1982).
- [27] B. K. Agrawal, S. Shlomo, and V. Kim Au, *Phys. Rev. C* **68**, 031304 (2003).
- [28] P.-G. Reinhard and H. Flocard, *Nucl. Phys. A* **584**, 467 (1995).
- [29] P. Klupfel, P.-G. Reinhard, T. J. Burvenich, and J. A. Maruhn, *Phys. Rev. C* **79**, 034310 (2009).
- [30] N. Lyutorovich, V. I. Tselyaev, J. Speth, S. Krewald, F. Grümmer, and P.-G. Reinhard, *Phys. Rev. Lett.* **109**, 092502 (2012).
- [31] E. Chabanat, P. Bonche, P. Haensel, J. Meyer, and R. Schaeffer, *Nucl. Phys. A* **635**, 231 (1998).
- [32] L. Bennour, P.-H. Heenen, P. Bonche, J. Dobaczewski, and H. Flocard, *Phys. Rev. C* **40**, 2834 (1989).
- [33] P.-G. Reinhard, D. J. Dean, W. Nazarewicz, J. Dobaczewski, J. A. Maruhn, and M. R. Strayer, *Phys. Rev. C* **60**, 014316 (1999).
- [34] L. G. Cao, U. Lombardo, C. W. Shen, and N. V. Giai, *Phys. Rev. C* **73**, 014313 (2006).
- [35] L.-W. Chen, C. M. Ko, B.-A. Li, and J. Xu, *Phys. Rev. C* **82**, 024321 (2010).
- [36] A. W. Steiner, M. Prakash, J. M. Lattimer, and P. J. Ellis, *Phys. Rep.* **411**, 325 (2005).
- [37] P. A. M. Guichon, H. H. Matevosyan, N. Sandulescu, and A. W. Thomas, *Nucl. Phys. A* **772**, 1 (2006).
- [38] F. Tondeur, M. Brack, M. Farine, and J. M. Pearson, *Nucl. Phys. A* **420**, 297 (1984).
- [39] B. A. Brown, G. Shen, G. C. Hillhouse, J. Meng, and A. Trzcinska, *Phys. Rev. C* **76**, 034305 (2007).
- [40] J. Friedrich and P.-G. Reinhard, *Phys. Rev. C* **33**, 335 (1986).
- [41] B. Cochet, K. Bennaceur, P. Bonche, T. Duguet, and J. Meyer, *Nucl. Phys. A* **731**, 34 (2004).
- [42] J. Piekarewicz, B. K. Agrawal, G. Colò, W. Nazarewicz, N. Paar, P.-G. Reinhard, X. Roca-Maza, and D. Vretenar, *Phys. Rev. C* **85**, 041302 (2012).
- [43] P.-G. Reinhard, J. Piekarewicz, W. Nazarewicz, B. K. Agrawal, N. Paar, and X. Roca-Maza, *Phys. Rev. C* **88**, 034325 (2013).
- [44] M. Vandebrouck, J. Gibelin, E. Khan, N. L. Achouri, H. Baba, D. Beaumel, Y. Blumenfeld, M. Caamaño, L. Caceres, G. Colò, F. Delaunay, B. Fernandez-Dominguez, U. Garg, G. F. Grinyer, M. N. Harakeh, N. Kalantar-Nayestanaki, N. Keeley, W. Mittig, J. Pancin, R. Raabe, T. Roger, P. Roussel-Chomaz, H. Savajols, O. Sorlin, C. Stodel, D. Suzuki, and J. C. Thomas, *Phys. Rev. Lett.* **113**, 032504 (2014).
- [45] D. H. Youngblood, Y.-W. Lui, and H. L. Clark, *Phys. Rev. C* **63**, 067301 (2001).
- [46] Y.-W. Lui, D. H. Youngblood, S. Shlomo, X. Chen, Y. Tokimoto, Krishichayan, M. Anders, and J. Button, *Phys. Rev. C* **83**, 044327 (2011).
- [47] Krishichayan, Y.-W. Lui, J. Button, D. H. Youngblood, G. Bonasera, and S. Shlomo, *Phys. Rev. C* **92**, 044323 (2015).
- [48] D. H. Youngblood, Y.-W. Lui, H. L. Clark, B. John, Y. Tokimoto, and X. Chen, *Phys. Rev. C* **69**, 034315 (2004).
- [49] D. H. Youngblood, Y.-W. Lui, and H. L. Clark, *Phys. Rev. C* **65**, 034302 (2002).
- [50] Y.-W. Lui, H. L. Clark, and D. H. Youngblood, *Phys. Rev. C* **61**, 067307 (2000).
- [51] D. H. Youngblood, Y.-W. Lui, and H. L. Clark, *Phys. Rev. C* **60**, 014304 (1999).
- [52] A. Veyssièrè, H. Beil, R. Bergère, P. Carlos, A. Leprêtre, and A. De Miniac, *Nucl. Phys. A* **227**, 513 (1974).
- [53] D. A. Sims, G. J. O'Keefe, R. P. Rassool, A. Kuzin, M. N. Thompson, J.-O. Adler, B.-E. Andersson, K. G. Fissum, K. Hansen, L. Isaksson, B. Nilsson, H. Ruijter, A. Sandell, B. Schröder, J. R. M. Annand, G. I. Crawford, P. D. Harty, J. C. McGeorge, and G. J. Miller, *Phys. Rev. C* **55**, 1288 (1997).
- [54] G. J. O'Keefe, M. N. Thompson, Y. I. Assafiri, R. E. Pywell, and K. Shoda, *Nucl. Phys. A* **469**, 239 (1987).
- [55] D. Rossi, P. Adrich, F. Aksouh, H. Alvarez-Pol, T. Aumann *et al.*, *Phys. Rev. Lett.* **111**, 242503 (2013).
- [56] B. L. Berman, J. T. Caldwell, R. R. Harvey, M. A. Kelly, R. L. Bramblett, and S. C. Fultz, *Phys. Rev.* **162**, 1098 (1967).
- [57] S. C. Fultz, B. L. Berman, J. T. Caldwell, R. L. Bramblett, and M. A. Kelly, *Phys. Rev.* **186**, 1255 (1969).
- [58] P. Carlos, H. Beil, R. Bergère, A. Leprêtre, A. De Miniac, and A. Veyssièrè, *Nucl. Phys. A* **225**, 171 (1974).
- [59] X. Roca-Maza, M. Brenna, B. K. Agrawal, P. F. Bortignon, G. Colò, L.-G. Cao, N. Paar, and D. Vretenar, *Phys. Rev. C* **87**, 034301 (2013).
- [60] A. Tamii, I. Poltoratska, P. von Neumann-Cosel, Y. Fujita, T. Adachi, C. A. Bertulani, J. Carter, M. Dozono, H. Fujita, K. Fujita, K. Hatanaka, D. Ishikawa, M. Itoh, T. Kawabata, Y. Kalmykov, A. M. Krumbholz, E. Litvinova, H. Matsubara, K. Nakanishi, R. Neveling, H. Okamura, H. J. Ong, B. Özel-Tashenov, V. Y. Ponomarev, A. Richter, H. Rubio, H. Sakaguchi, Y. Sakemi, Y. Sasamoto, Y. Shimbara, Y. Shimizu,



- F. D. Smit, T. Suzuki, Y. Tameshige, J. Wambach, R. Yamada, M. Yosoi, and J. Zenihiro, *Phys. Rev. Lett.* **107**, 062502 (2011).
- [61] J. P. Blaizot, *Phys. Rep.* **64**, 171 (1980).
- [62] U. Garg, and G. Colò, *Prog. Part. Nucl. Phys.* **101**, 55 (2018).
- [63] H. L. Clark, Y.-W. Lui, and D. H. Youngblood, *Phys. Rev. C* **63**, 031301 (2001).
- [64] G. Colò, N. Van Giai, P. F. Bortignon, and M. R. Quaglia, *Phys. Lett. B* **485**, 362 (2000).
- [65] D. Vretenar, A. Wandelt, and P. Ring, *Phys. Lett. B* **487**, 334 (2000).
- [66] M. R. Anders, S. Shlomo, T. Sil, D. H. Youngblood, Y.-W. Lui, and Krishichayan, *Phys. Rev. C* **87**, 024303 (2013).
- [67] H. Krivine, J. Treiner, and O. Bohigas, *Nucl. Phys. A* **336**, 155 (1980).
- [68] C. J. Horowitz, E. F. Brown, Y. Kim, W. G. Lynch, R. Michaels, A. Ono, J. Piekarewicz, M. B. Tsang, and H. H. Wolter, *J. Phys. G Nucl. Part. Phys.* **41**, 093001 (2014).